



J. Plankton Res. (2021) 1–21. doi:10.1093/plankt/fbab028

BLOOFINZ - Gulf of Mexico

Taxon-specific phytoplankton growth, nutrient utilization and light limitation in the oligotrophic Gulf of Mexico

NATALIA YINGLING^{1,*}, THOMAS B. KELLY¹, TAYLOR A. SHROPSHIRE¹, MICHAEL R. LANDRY², KAREN E. SELPH³, ANGELA N. KNAPP¹, SVEN A. KRANZ¹ AND MICHAEL R. STUKEL¹

¹DEPARTMENT OF EARTH, OCEAN AND ATMOSPHERIC SCIENCE, FLORIDA STATE UNIVERSITY, TALLAHASSEE, FL 32306, USA, ²SCRIPPS INSTITUTION OF OCEANOGRAPHY, 9500 GILMAN DR., LA JOLLA, CA 92093-0227, USA AND ³DEPARTMENT OF OCEANOGRAPHY, UNIVERSITY OF HAWAII AT MANOA, HONOLULU, HI 96822, USA

*CORRESPONDING AUTHOR: ny18b@my.fsu.edu

Received October 21, 2020; editorial decision March 1, 2021; accepted March 23, 2021

Corresponding editor: Pia Moisander

The highly stratified, oligotrophic regions of the oceans are predominantly nitrogen limited in the surface ocean and light limited at the deep chlorophyll maximum (DCM). Hence, determining light and nitrogen co-limitation patterns for diverse phytoplankton taxa is crucial to understanding marine primary production throughout the euphotic zone. During two cruises in the deep-water Gulf of Mexico, we measured primary productivity ($H^{13}CO_3^-$), nitrate uptake ($^{15}NO_3^-$) and ammonium uptake ($^{15}NH_4^+$) throughout the water column. Primary productivity declined with depth from the mixed layer to the DCM, averaging $27.1 \text{ mmol C m}^{-2} \text{ d}^{-1}$. The fraction of growth supported by NO_3^- was consistently low, with upper euphotic zone values ranging from 0.01 to 0.14 and lower euphotic zone values ranging from 0.03 to 0.44. Nitrate uptake showed strong diel patterns (maximum during the day), whereas ammonium uptake exhibited no diel variability. To parameterize taxon-specific phytoplankton nutrient and light utilization, we used a data assimilation approach (Bayesian Markov Chain Monte Carlo) including primary productivity, nutrient uptake and taxon-specific growth rate measurements. Parameters derived from this analysis define distinct niches for five phytoplankton taxa (*Prochlorococcus*, *Synechococcus*, diatoms, dinoflagellates and prymnesiophytes) and may be useful for constraining biogeochemical models of oligotrophic open-ocean systems.

KEYWORDS: new production; recycled production; half-saturation; photosynthesis–irradiance; nutrient kinetics

INTRODUCTION

Nutrient acquisition by phytoplankton is an important factor regulating marine primary productivity (Davey *et al.*, 2008; Duce *et al.*, 2008; Mulholland and Lomas, 2008). The open-ocean Gulf of Mexico (GoM) is a highly stratified, oligotrophic region where the Loop Current, mesoscale eddies and episodic storm events influence lateral and vertical transport of nutrients and organisms (Biggs, 1992; Forristall *et al.*, 1992; Biggs and Ressler, 2001; Oey *et al.*, 2005). These features create dynamic ecological mosaics with substantial mesoscale spatial variability in the phytoplankton community (Biggs and Müller-Karger, 2008; Gomez *et al.*, 2018). Intense stratification also leads to deep chlorophyll maxima (DCM) that potentially provide unique niches for phytoplankton compared with low-nutrient, high-light environments found in the shallow mixed layer (Shropshire *et al.*, 2020; Knapp *et al.*, 2021; Selph *et al.*, 2021). Additionally, the oligotrophic GoM is an important spawning region for economically valuable and environmentally important nekton, including Atlantic Bluefin Tuna (Rooker *et al.*, 2007; Cornic *et al.*, 2018). In addition to vertical advection, previous studies have found that nitrogen fixation, NO_3^- upwelling along the boundaries of mesoscale eddies and horizontal advection of nutrients can be important nitrogen sources in the GoM (Walker *et al.*, 2005; Mulholland *et al.*, 2006). While the sources of bioavailable nitrogen in the oligotrophic GoM are likely spatiotemporally variable, a more accurate understanding of phytoplankton nutrient-uptake dynamics is important to provide insight into what regulates group-specific community composition and inform future biogeochemical models.

Variability in phytoplankton ecophysiology adds complexity to the basic processes of primary productivity in pelagic habitats. *Prochlorococcus* is often the dominant phytoplankton taxon in oligotrophic regions (Chisholm *et al.*, 1988; Partensky *et al.*, 1999); however, many ecotypes of this genus exist, with different nutrient uptake capabilities and consequently biogeochemical impacts (Zwirgmaier *et al.*, 2008; Martiny *et al.*, 2009; Kashtan *et al.*, 2014; Kent *et al.*, 2016; De Martini *et al.*, 2018). *Prochlorococcus* is the numerically dominant phytoplankton in our study region and comprises roughly half of the total carbon-based biomass (Selph *et al.*, 2021). *Synechococcus* and picoeukaryotes (especially prymnesiophytes, chlorophytes and pelagophytes) are also important, with picoeukaryotes comprising a larger portion of biomass with increasing depth (Selph *et al.*, 2021). Since different phytoplankton groups, as well as species and ecotypes within groups, differ in their adaptations for life in nutrient-depleted environments,

their responses to dynamic environments may also be quantitatively and qualitatively different (Dutkiewicz *et al.*, 2013).

Constraining phytoplankton functional relationships (i.e. phytoplankton responses to environmental variables) is necessary to enable forecasting of ecological impacts in dynamic environments and modified physical conditions—such as those expected in a future ocean. Numerical modeling of marine microbial ecosystems is presently limited by an inability to accurately constrain *in situ* ecophysiological relationships among diverse phytoplankton taxa (Anderson, 2005; Franks, 2009; Follows and Dutkiewicz, 2011). Here, we address three questions aiming to better constrain group-specific functional phytoplankton relationships: (i) how do net primary production (NPP) and NO_3^- uptake rates of phytoplankton in the open-ocean GoM vary with depth and time of day; (ii) what nitrogen sources support these phytoplankton and (iii) how do nutrient limitation and light limitation vary among different phytoplankton taxa?

Answers to these questions are derived from measurements collected during two field studies as part of the Bluefin Larvae in Oligotrophic Ocean Foodwebs: Investigating Nutrients to Zooplankton in the Gulf of Mexico (BLOOFINZ-GoM) project (Gerard *et al.*, 2021). Specifically, we conducted Lagrangian experiments with repeated depth-resolved measurements of NPP, nutrient uptake and taxon-specific phytoplankton growth rates, while also assessing the biomass of different phytoplankton. We then assimilate the field data to parameterize group-specific phytoplankton nutrient kinetics for application to biogeochemical models.

METHODS

Cruise structure and sampling strategy

Data are from two cruises in the open-ocean northern GoM (NF1704 in May, 2017; NF1802 in May 2018) as part of the BLOOFINZ-GoM project. We conducted five Lagrangian experiments (“Cycles” referred to as C1, C2, C3, C4 and C5 to represent each cycle) lasting 2–4 days each (Gerard *et al.*, 2021). Each cycle used a pair of satellite-tracked marker buoys tethered to subsurface drogues to follow the mixed layer in a Lagrangian frame of reference (Landry *et al.*, 2009; Stukel *et al.*, 2015). One array (“incubation array”) included attachment points for mesh bags containing incubation bottles for NO_3^- uptake, NPP and taxon-specific phytoplankton growth and grazing rates at depths spanning the euphotic zone. The Lagrangian approach permitted repeated sampling of the same water parcel to quantify variability in

phytoplankton biomass and rates over the duration of each cycle. Samples for fluorometric chlorophyll *a* (Strickland and Parsons, 1972), phytoplankton biomass (Selph *et al.*, 2021), nutrients (NO_3^- and NH_4^+ , Knapp *et al.*, 2021) and *in situ* incubation experiments were collected at six depths from the surface to the DCM on daily 02:00 a.m. (local US central) CTD-Niskin rosette casts. Samples for shipboard incubations were collected from daily CTD casts near dusk. For more detail on sampling methodology see the aforementioned studies in this issue.

Phytoplankton community composition and biomass

As reported in Selph *et al.* (2021), we quantified phytoplankton abundance using a combination of flow cytometry (FCM), epifluorescence microscopy (EPI) and high-pressure liquid chromatography (HPLC). Cells identified by FCM were categorized into three populations [*Prochlorococcus* (PRO), *Synechococcus* (SYN) and picoeukaryotes (PEUK)] based on forward-angle and side-angle light scattering and fluorescence signatures for DNA, phycoerythrin and chlorophyll. For larger cells [i.e. diatoms (DIAT), autotrophic dinoflagellates (ADINO), prymnesiophytes (PRYM)] and other eukaryotes (OTHER), a combination of HPLC and EPI was used to determine taxa-specific biomass. HPLC-derived pigments were partitioned into taxonomic groups using CHEMTAX (Wright 2008; Higgins *et al.*, 2011; Selph *et al.*, 2021). EPI samples from the shallowest two depths [within the mixed layer, which we define as the depth at which density increases by 0.125 kg/m^{-3} (Monterey and Levitus, 1997)] and the deepest two depths (just above and at the DCM) from three of the Lagrangian cycles (C1, C4 and C5) were used to determine depth-varying carbon:chlorophyll ratios, hence, carbon-based biomass for each group. Assuming Redfield C:N ratios (106:16, mol:mol), carbon-based biomasses from Selph *et al.* (2021) were converted to nitrogen-based biomasses for the biogeochemical model (Redfield *et al.* 1963). See Supplemental Material A1 and Selph *et al.* (2021) for additional details.

Phytoplankton growth, productivity and grazing rates

We used three distinct incubation strategies for quantifying phytoplankton productivity and nutrient uptake rates: 24-h *in situ* incubations on the “incubation” array (NPP, NO_3^- uptake and taxon-specific phytoplankton growth rates); 6-h shipboard incubations starting at dawn (vertical patterns of NO_3^- and NH_4^+ uptake) and diel shipboard

incubations consisting of sequential 4-h incubations for 24-h (diurnal patterns of NO_3^- and NH_4^+ uptake).

Taxon-specific growth rates

Two-point seawater dilution grazing experiments were conducted *in situ* daily at six depths spanning the euphotic zone to determine taxon-specific phytoplankton growth rates for a total of 88 independent experiments (Landry *et al.*, 2008, 2011, 2021). In total, 2.7-L samples of either whole seawater or partially diluted seawater (32% whole seawater/68% 0.1- μm filtered seawater) were incubated for 24-h on the incubation array. Initial and final samples for FCM (*Prochlorococcus* and *Synechococcus*), HPLC (dinoflagellates, diatoms and prymnesiophytes) and fluorometric chlorophyll *a* (bulk phytoplankton) were used to determine taxon-specific phytoplankton growth and mortality at each depth. See Supplemental Material A1 and Landry *et al.* (2021) for additional details.

In situ NPP and nitrate uptake

NPP and $^{15}\text{NO}_3^-$ uptake rates were measured at the same six depths on the incubation array. Four incubation bottles (2.7 L) per depth were filled from Niskin rosettes (three light bottles, one dark bottle). All bottles were spiked with $\text{H}^{13}\text{CO}_3^-$ (final concentration of 154 or 196 $\mu\text{mol L}^{-1}$ on NF1704 and NF1802, respectively). Two light bottles were spiked with $^{15}\text{NO}_3^-$ (final concentration of 10 or 8 nmol L^{-1} on NF1704 and NF1802, respectively). Bottles were then incubated for 24-h on the array. Upon recovery, incubations were immediately vacuum filtered onto pre-combusted 25-mm GF/F filters in the dark. Filters were rinsed with filtered seawater, wrapped in foil and stored at -80°C . Samples were fumigated with HCl vapor to remove inorganic carbon, dried and placed inside a tin cup to be used for C/N and isotopic analysis at the University of California, Davis stable isotope facility. Uptake rates ($^{15}\text{NO}_3^-$ or bicarbonate) were determined for each incubation bottle using equations in Stukel (2020). NO_3^- uptake is reported as the average and uncertainty of the $^{15}\text{NO}_3^-$ spiked bottles. As no statistically significant difference in $\text{H}^{13}\text{CO}_3^-$ uptake was detected between bottles spiked with $^{15}\text{NO}_3^-$ and those without, NPP is reported as the average and uncertainty of $\text{H}^{13}\text{CO}_3^-$ uptake in the three light bottles corrected for dark bottle $\text{H}^{13}\text{CO}_3^-$ uptake.

Shipboard vertically resolved nitrate and ammonium uptake

Since NH_4^+ recycling within 24-h bottle incubations can substantially bias measurements of NH_4^+ uptake (Dugdale and Wilkerson, 1986), we conducted short-term (6-h)

NH_4^+ and NO_3^- uptake experiments in shipboard incubators. Each incubator was uniformly shaded using clear or blue-tinted acrylic sheets to achieve three light levels as determined by simultaneous measurements with a $2\text{-}\pi$ LI-COR photosynthetically active radiation (PAR) sensor for downwelling irradiance and a $4\text{-}\pi$ water-proof LI-COR PAR sensor for ambient irradiance in the incubator. These calibrations were done shipboard to account for light reflection or shading effects specific to their location. Incubation light levels for NF1704 (C1–C3) were determined to be 145% (clear, surface), 79% (mixed layer) and 21% (lower mixed layer) of surface irradiance (I_0). For NF1802 (C4–C5), the clear incubator was replaced with one screened to 1.7% I_0 to mimic DCM light. Incubators were cooled with mixed-layer seawater (24.5–26.5°C). Samples were drawn from depths near these light levels (as determined from noon CTD casts with CTD-mounted PAR sensor).

To determine patterns of nitrate and ammonium uptake as a function of depth, six 2.7-L samples from each of the three incubator light levels (e.g. 5, 15 and 45 m for surface, 79% and 21% I_0 , respectively) were collected near dusk and placed in the incubators until dawn (N.B., ship schedule and CTD water budget did not allow dawn sampling for these experiments). At dawn, triplicate samples from each depth were spiked with either $^{15}\text{NO}_3^-$ or $^{15}\text{NH}_4^+$ (concentrations as above) and incubated for 6-h (dawn to approximately local noon). Samples were then filtered and analyzed as described above.

Shipboard diel nitrate and ammonium uptake experiments

To determine diel variability in nutrient uptake and assess potential recycling occurring within 24-h incubations, we also conducted short-term (diurnally resolved) nutrient uptake experiments. Nine to twelve 2.7-L bottles were filled at dusk. Two or three 24-h reference bottles (24-h incubation) and an additional “time point” bottle (4-h incubation) were immediately spiked with $^{15}\text{NO}_3^-$ or $^{15}\text{NH}_4^+$ (the remainder of the bottles were not immediately spiked). All bottles were then returned to the incubator. After ~4-h, the first experimental bottle was removed from the incubator and filtered, and a second experimental bottle was spiked. This process continued for 24-h to produce six sequential 4-h incubations from which diurnal patterns of nutrient uptake could be determined. After 24-h, the reference bottles were harvested. No diel experiments were conducted during C3 (NF1704), and no diel ammonium uptake experiments were conducted during C4 (NF1802). On all other cycles (C1, C2, C5), simultaneous NO_3^- or NH_4^+ uptake diel experiments were conducted. On NF1802 (C4–C5), diel experiment

bottles were also spiked with $\text{H}^{13}\text{CO}_3^-$ to simultaneously determine diel variability in NPP.

Data assimilation and model parameterization

Model structure

Phytoplankton growth is parameterized using transfer functions from the biogeochemical model NEMURO-GoM (Shropshire *et al.*, 2020; Shropshire *et al.*, 2021), which was designed for the open-ocean GoM. NEMURO-GoM parameterizes phytoplankton growth as a function of light, nutrients and temperature. By default, it includes two phytoplankton groups [small (SP) and large (LP)]; however, we extended this model to parameterize six distinct groups that were identifiable through FCM, HPLC and/or EPI approaches above: (i) PRO, (ii) SYN, (iii) PRYM, (iv) ADINO, (v) DIAT and (vi) OTHER (equaling the residual biomass from the remaining groups of autotrophic eukaryotic phytoplankton).

NEMURO-GoM parameterizes group-specific growth rates with the following seven equations: (i) NO_3^- limitation (NL), (ii) NH_4^+ limitation (AL), (iii) light limitation (LL), (iv) temperature limitation (TL), (v) respiration (Resp.), (vi) gross primary productivity and (vii) NPP, wherein K_{NO_3} is the NO_3^- half-saturation constant (μM), K_{NH_4} is the NH_4^+ half-saturation constant (μM), α is the initial slope of the photosynthesis-vs-irradiance curve ($\text{m}^2 \text{W}^{-1} \text{d}^{-1}$), β is the light-inhibition constant ($\text{m}^2 \text{W}^{-1} \text{d}^{-1}$) and V is the maximum specific growth rate at a reference temperature (d^{-1}). NEMURO-GoM uses a reference temperature of 0°C, but we provide values referenced to 25°C, which is representative of the GoM mixed layer during our cruises. Q is the temperature effect coefficient ($^{\circ}\text{C}^{-1}$), R is biomass-specific respiration, E is growth-specific excretion and B is biomass (mmol N m^{-3}). Subscript “ i ” indicates group-specific parameters with nitrate concentrations [μM , (NO_3^-)], ammonium concentrations [μM , (NH_4^+)], PAR and T ($^{\circ}\text{C}$) as environmental conditions. For our Bayesian parameter-selection procedure (see below), all group-specific parameters except β were log transformed. Equations are as follows:

$$NL_i = \frac{[\text{NO}_3^-]}{[\text{NO}_3^-] + K_{\text{NO}_3,i}} \cdot \left(1 + \frac{[\text{NH}_4^+]}{K_{\text{NH}_4,i}}\right)^{-1} \quad (1)$$

$$AL_i = \frac{[\text{NH}_4^+]}{[\text{NH}_4^+] + K_{\text{NH}_4,i}} \quad (2)$$

$$LL_i = \left(1 - \exp\left(\frac{-\alpha_i \cdot \text{PAR}}{V_i}\right)\right) \cdot \exp\left(\frac{-\beta_i \cdot \text{PAR}}{V_i}\right) \quad (3)$$

$$TL_i = \exp(Q \cdot T) \quad (4)$$

Table I: Summary of data for each Lagrangian cycle

	Cycle 1	Cycle 2	Cycle 3	Cycle 4	Cycle 5
Surface NO ₃ ⁻ (μM)	<0.1	<0.1	<0.1	<0.1	<0.1
Surface NH ₄ ⁺ (μM)	<0.025	<0.025	<0.025	<0.025	0.025
Surface Chl <i>a</i> (μg/L)	0.107 ± 0.04	0.049	0.080 ± 0.007	0.100 ± 0.01	0.127 ± 0.01
NPP (mmol C m ⁻² d ⁻¹)	25.6 ± 0.1	24.4 ± 2.8	24.9 ± 0.4	29.2 ± 3.0	30.1 ± 2.9
<i>In situ</i> NO ₃ ⁻ uptake (μmol N m ⁻² d ⁻¹)	3.45 ± 1.63	1.49 ± 0.21	0.99 ± 0.37	0.74 ± 0.02	1.48 ± 0.09
<i>f</i> -ratio	0.22	0.02	0.05	0.06	0.12

Surface NO₃⁻ and NH₄⁺ are averaged across days within a cycle. NPP, NO₃⁻ and *f*-ratio are vertically integrated values. *f*-ratio = NO₃⁻ uptake/(NH₄⁺ uptake + NO₃⁻ uptake) is a blended product that combines shipboard NO₃⁻ and ammonium uptake experiments (more accurate) with *in situ* NO₃⁻ uptake and NPP measurements (greater depth resolution).

$$Resp_i = R_i \cdot \exp(Q \cdot T) \quad (5)$$

$$GPP_i = V_i \cdot B_i \cdot (NL_i + AL_i) \cdot LL_i \cdot TL_i \quad (6)$$

$$NPP_i = GPP_i \cdot (1 - E_i) - Resp_i \cdot B_i \quad (7)$$

Bayesian parameter optimization procedure

To constrain group-specific model parameters, we used a Bayesian parameter-selection method applied to a modified 0-dimensional version of NEMURO-GoM consisting of equations 1–7 with six phytoplankton taxa (additional details in Supplemental Material A2). Our objective was not to find a single “best” parameterization, but rather to develop a statistical ensemble of possible parameter sets that reflects both uncertainty within the data and uncertainty in taxon-specific responses to light, temperature and nutrients. Briefly, the initial parameter set, τ_0 , is set to be equivalent to NEMURO-GoM default parameterizations for either SP or LP (Supplemental Table SI). The model is then initialized and run with *in situ* phytoplankton abundances, nutrient concentrations, temperature and light equivalent to the observed initial conditions for every *in situ* incubation experiment. A joint probability is then used to assess both the model-data misfit (sum-of-squared normalized residuals) between observations (NPP, NO₃⁻ uptake and taxon-specific growth rates) and model results (equation 8; “likelihood”) and the prior probability of the parameter set used (equation 9).

$$\text{Likelihood} : P(\text{data}|\tau) = \prod_{i \in \text{data}} \left(\frac{1}{\sigma_i \sqrt{2\pi}} \cdot e^{-\frac{1}{2} \left(\frac{x_i - x'_i}{\sigma_i} \right)^2} \right) \quad (8)$$

where x_i and σ_i are the measurement and measurement uncertainty, respectively, of the i th observation and x'_i is

the modeled value for that observation.

$$\text{Prior probability} : P(\tau) = \prod_{i \in \tau} \left(\frac{1}{\sigma_i \sqrt{2\pi}} \cdot e^{-\frac{1}{2} \left(\frac{t - t^*}{\sigma_i} \right)^2} \right) \quad (9)$$

where t^* and σ_i are the mean and standard deviation (SD), respectively, for the prior estimate of model parameter value t (Supplemental Table SI).

To explore the possible solution space, we used a Markov Chain Monte Carlo procedure with the Metropolis–Hastings algorithm (Hastings, 1970). For each iteration of the random walk, each parameter is varied by a small increment (in log-transformed space if a variable was transformed) yielding a new parameter set: τ_{j+1} , which is used to rerun the model yielding a new likelihood and prior probability. The new parameter set would be “accepted” any time cost [i.e. $-P(\text{data}|\tau_{j+1}) \cdot P(\tau_{j+1})$] decreased and may be accepted even when cost increases based on the acceptance ratio: $\frac{-P(\text{data}|\tau_{j+1}) \cdot P(\tau_{j+1})}{-P(\text{data}|\tau_j) \cdot P(\tau_j)}$. If the new parameter set

is accepted, the random walk continues from τ_{j+1} . Otherwise a new τ_{j+1} is calculated. The first 50% of accepted parameter sets were removed (“burn-in”) and the remainder were subsampled (1 in 50) to remove autocorrelation between parameter sets and yielding ~ 20 000 final parameter sets.

RESULTS

In situ conditions and the phytoplankton community

All five cycles had surface chlorophyll concentrations < 0.2 μg L⁻¹ and a pronounced DCM between 69 and 137 m (Gerard et al., 2021). The top of the DCM typically corresponded to ~ 1–2% I_0 . NO₃⁻ concentrations were consistently < 0.1 μM at depths shallower than 69 m

Table II: Summary of *in situ* observations

	Cycle 1	Cycle 2	Cycle 3	Cycle 4	Cycle 5
<i>Prochlorococcus</i>	6.16 ± 0.22	6.76 ± 0.28	6.85 ± 0.37	4.85 ± 0.04	3.24 ± 0.45
<i>Synechococcus</i>	1.44 ± 0.04	1.25 ± 0.03	1.22 ± 0.04	2.57 ± 0.05	2.36 ± 0.37
Diatom	0.26 ± 0.11	NM	NM	0.07 ± 0.004	0.04 ± 0.003
Dinoflagellate	0.47 ± 0.05	NM	NM	0.40 ± 0.11	0.43 ± 0.02
Prymnesiophytes	0.33 ± 0.03	NM	NM	0.44 ± 0.18	0.54 ± 0.03
Other eukaryotes	2.46 ± 0.84	0.79 ± 0.0	0.60 ± 0.0	0.47 ± 0.11	1.64 ± 0.5

Group-specific biomass are vertically integrated to the base of the euphotic zone for each Lagrangian cycle. Units are mmol N m⁻² (converted from carbon-based values reported in Selph *et al.* (2021) by dividing by a Redfield C:N ratio of 106:16, mol:mol). Values marked with NM were not measured.

and generally <1 μM throughout the entire euphotic zone (Knapp *et al.*, 2021). Only C5, with the shallowest euphotic zone and closest to the shelf break, had > 1 μM NO₃⁻ at <100 m depth. A summary of surface NO₃⁻, NH₄⁺ and chlorophyll concentrations along with vertically integrated NPP, NO₃⁻ and *f*-ratio can be found in Table I.

Prochlorococcus averaged ~50% of the carbon-based phytoplankton biomass in all water parcels, although its proportional contribution varied from 31 to 66% of integrated euphotic zone biomass, being slightly more dominant in cycles with deeper DCMs (Table II). PRO biomass typically increased with depth from the mixed layer to a subsurface maximum slightly above the DCM before declining at the DCM. Mixed-layer SYN:PRO biomass ratios ranged from 0.2 to 1.4. However, SYN biomass decreased with depth, such that it represented ≤10% of PRO biomass at the DCM. Combined, cyanobacteria contributed a mean (±SD) of 67 ± 14% of euphotic zone integrated autotrophic carbon, whereas 2–10-μm eukaryotic cells comprised most of the remaining biomass. Prymnesiophytes were the dominant eukaryotic taxa, comprising 17 ± 7%, whereas chlorophytes and pelagophytes represented 5 ± 3% and 4.2 ± 2%, respectively, of integrated euphotic zone carbon biomass. Diatoms were only minor contributors to autotrophic biomass (<2% in all cycles). For additional details on community composition, see Selph *et al.* (2021).

Vertical profiles of NPP and nutrient uptake

NPP declined almost monotonically with depth on all cycles, although mixed-layer NPP was typically only 2–3-fold higher than NPP at the DCM (Fig. 1). NPP showed relatively weak intercycle variability. Cycle-average NPP varied from 0.27 to 0.55 μmol C L⁻¹ d⁻¹ at 5 m and varied from 0.10 to 0.29 μmol C L⁻¹ d⁻¹ at the DCM. The highest vertically integrated NPP (mean: 29.3 mmol C m⁻² d⁻¹) was for C5 (the cycle closest to the shelf), which also had the shallowest DCM, euphotic zone

depth and nitracline. The lowest vertically integrated NPP was measured during C2 (24.3 mmol C m⁻² d⁻¹).

Vertical structure was less distinct for NO₃⁻ uptake rates (Fig. 1). Across depths and cycles, NO₃⁻ uptake typically ranged from 5 to 20 nmol N L⁻¹ d⁻¹. C1 exhibited a modest subsurface peak at 20–30 m (the rate was much higher for one outlier experiment at the DCM, likely due to contamination). C2 and C3 showed evidence for a weak subsurface maximum at ~60 m, whereas rates were relatively constant with depth for C4. C5 was the only cycle with a clear surface maximum in NO₃⁻ uptake rates. Vertically integrated, cycle-average NO₃⁻ uptake ranged from 0.72 (C4) to 3.45 mmol N m⁻² d⁻¹ (C1).

To investigate the relative proportion of NPP supported by NO₃⁻ uptake (commonly referred to as the *f*-ratio), we computed an *f*-ratio from *in situ* data as:

$$f_{is} = \frac{NO_3 \text{ Uptake}}{NPP/S}$$

where *S* is Redfield C:N stoichiometry (106:16). We caution that while *f*_{is} is similar to the commonly used *f*-ratio (proportion of N uptake provided by NO₃⁻), it should not be interpreted as equivalent to the technical definition of the *f*-ratio (new production divided by total production), because we suspect that nitrification in the euphotic zone may have been significant (Kelly *et al.*, in review; Stukel *et al.* in press). Furthermore, *f*_{is} may overestimate an *f*-ratio calculated from NO₃⁻ and NH₄⁺ uptake (see below), if phytoplankton engage in luxury nutrient uptake. With those caveats, vertically integrated, cycle-average *f*_{is} ranged from 0.17 to 0.89; however, the high value (0.89 from C1) was heavily biased by the aforementioned high NO₃⁻ uptake outlier at the DCM. If the results from this day's experiments are excluded, *f*_{is} for this cycle decreases to 0.47. Across all cycles, *f*_{is} generally increased with depth in the euphotic zone. It is important to note that heterotrophic bacteria may play a role in nutrient uptake; however, the data suggest that ammonium uptake was vertically correlated with NPP and phytoplankton growth rates (i.e. ammonium uptake

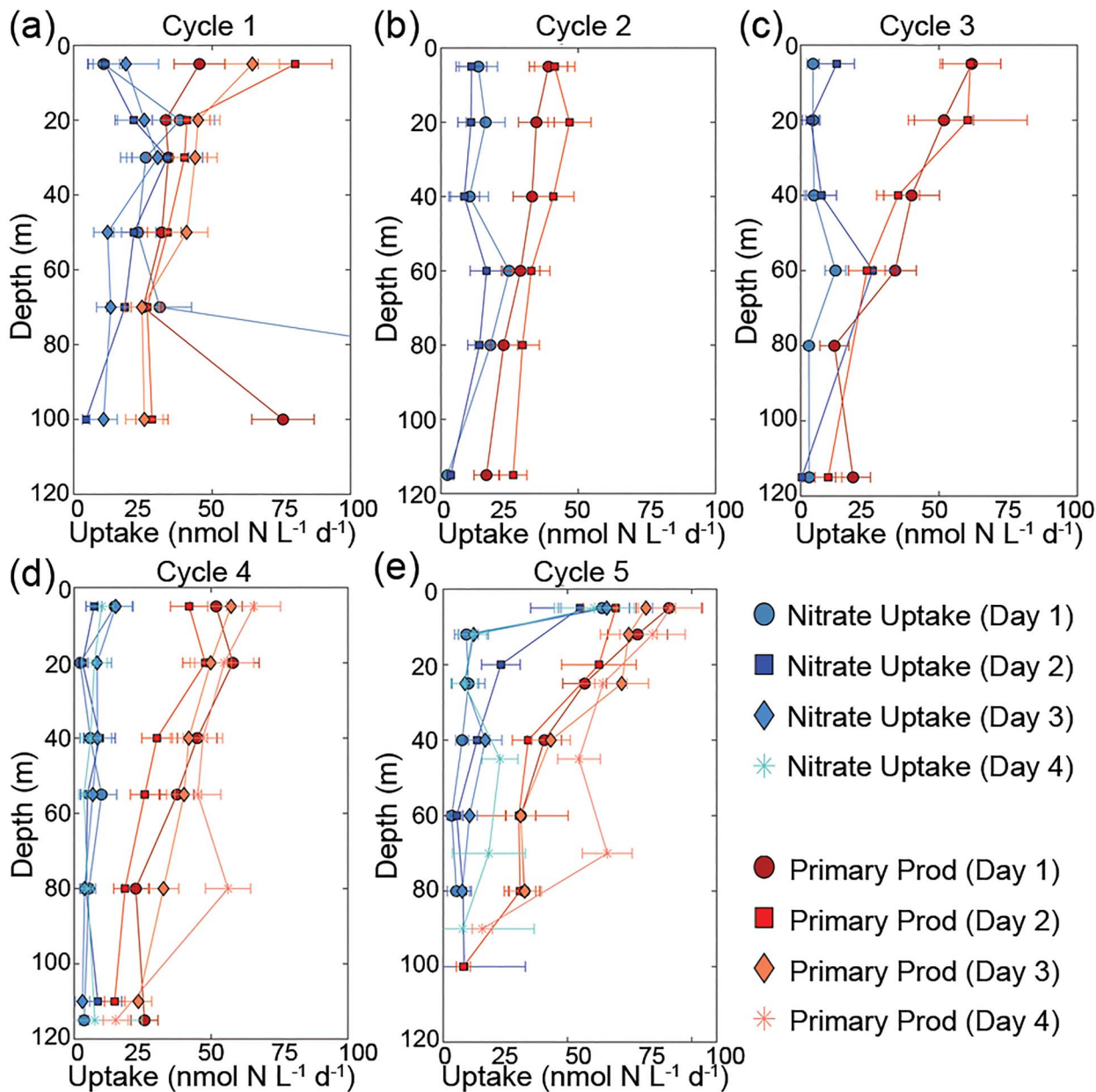


Fig. 1. NO_3^- (red) and HCO_3^- uptake (blue) rates from *in situ* incubations from (a) cycle 1, (b) cycle 2, (c) cycle 3, (d) cycle 4 and (e) cycle 5. HCO_3^- uptake rates are converted to nitrogen units assuming Redfield ratio (6.625 molar ratios of C:N). Error bars represent 1 SD of the mean.

was low at the light-limited DCM), whereas nitrate uptake was negligible during the night. Since community nitrate and ammonium uptake were light limited, we suspect that the majority of nutrient uptake was mediated by phytoplankton.

Shipboard, depth-resolved NO_3^- and NH_4^+ uptake experiments showed that NH_4^+ uptake is consistently higher than NO_3^- uptake for all cycles and depths (Fig. 2). Similar to the findings from *in situ* experiments, the data suggest that NH_4^+ is the preferred nitrogen

source. Experiments during 2017 (mixed-layer only) showed little variability with depth, although NO_3^- uptake was higher in C1 than C2 (as suggested by f_{is}). NO_3^- and NH_4^+ uptake rates from 2018 (which extended to the depth of the DCM) showed that NH_4^+ uptake was lower at the DCM than in the mixed-layer, a finding that also agrees with our *in situ* NPP results. Shipboard incubation-based f -ratios [$f_{deck} = \text{NO}_3^- \text{ uptake} / (\text{NO}_3^- \text{ uptake} + \text{NH}_4^+ \text{ uptake})$] were lower than f_{is} and ranged from 0.02 to 0.17. For

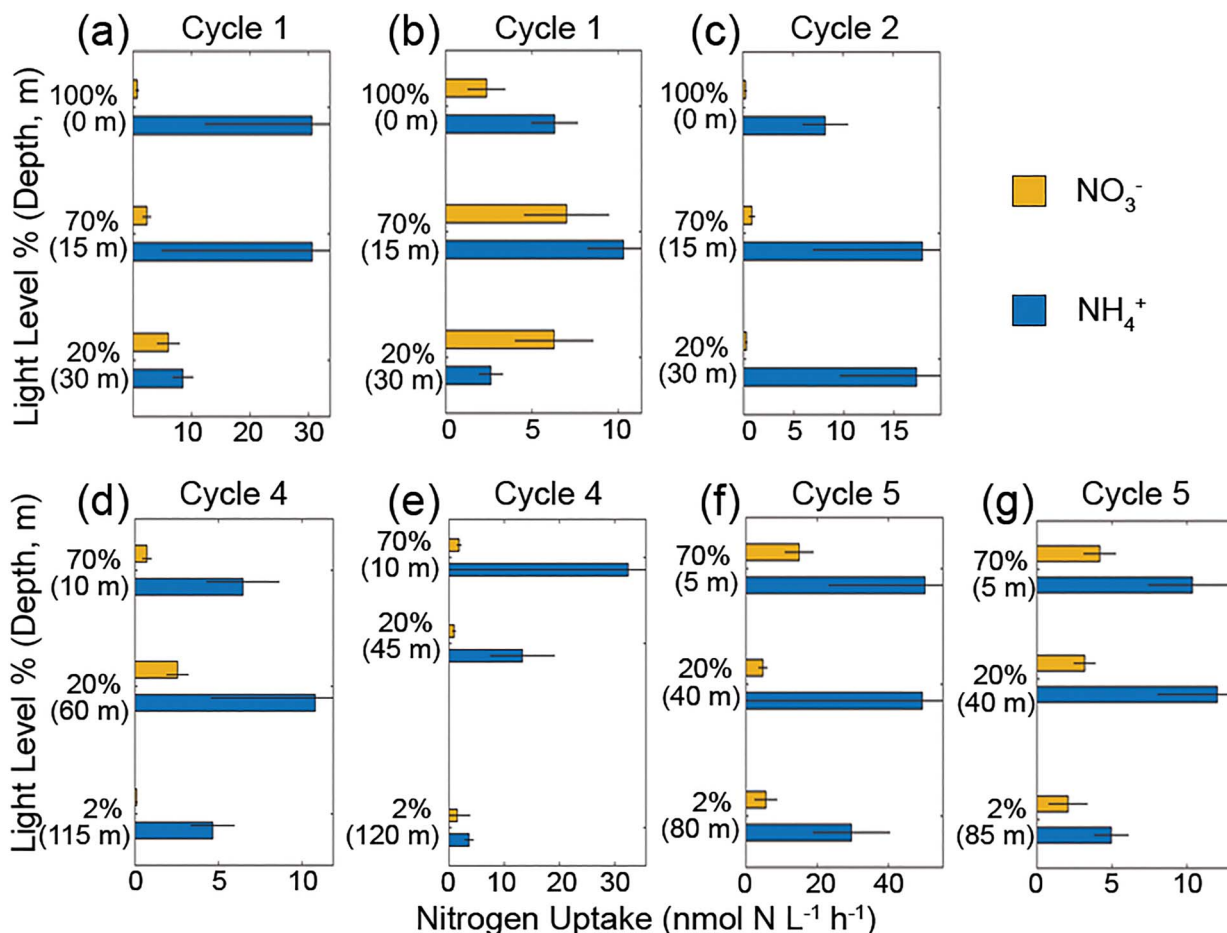


Fig. 2. Results from NO_3^- (blue) and NH_4^+ (orange) uptake experiments conducted shipboard at three light levels and water collection depth (m) as indicated. Panels (a) and (b) represent cycle 1, panel (c) represents cycle 2, panels (d) and (e) represent cycle 4 and panels (f) and (g) represent cycle 5. Error bars are replicate measurements.

f_{deck} , we assumed that NH_4^+ uptake occurs at constant rates over the full 24-h daily period (and hence multiplied 6-h experiments by 4), but that NO_3^- uptake occurs only during the day (hence multiplied 6-h experiments by 2), based on the results of diel experiments (next section). Because f_{deck} calculated from NO_3^- and NH_4^+ uptake measurements should be considered more accurate due to the shorter incubation times with less recycling occurring, we developed a blended f -ratio product: we treated f_{deck} as more accurate at paired depths but used the vertical patterns from f_{is} . That is, we multiplied f_{is} by the ratio of $f_{\text{deck}}:f_{\text{is}}$ at the nearest depths. This approach suggested that euphotic zone-averaged f -ratios varied from 0.02 to 0.22 (mean = 0.06). f -ratios were slightly higher in the deep euphotic zone (>50 m depth, f ranged from 0.03 to 0.44, mean = 0.14) than in the shallow euphotic zone ($f = 0.01$ –0.14, mean = 0.06).

Diel variability in NPP and nutrient uptake

Distinct patterns emerged from the sequential 4-h incubations assessing diel variability in NH_4^+ uptake (Fig. 3), NO_3^- uptake (Fig. 4) and NPP (Fig. 5). NO_3^- uptake and NPP were strongly light dependent, with consistent midday peaks and low activity during the night (Figs 4 and 5). However, NH_4^+ uptake showed no distinct diel patterns, with uptake rates as high at night as during the day. Comparison to simultaneous 24-h incubations allowed us to assess potential nutrient recycling in the euphotic zone. For NPP, the sum of six sequential 4-h $\text{H}^{13}\text{CO}_3^-$ uptake experiments were generally not significantly different from the mean of simultaneous 24-h uptake experiments, as expected, indicating that the time scale of $\text{H}^{13}\text{CO}_3^-$ recycling within the euphotic zone is long relative to the duration of a 24-h experiment. However, for both NO_3^- uptake and NH_4^+ uptake rates,

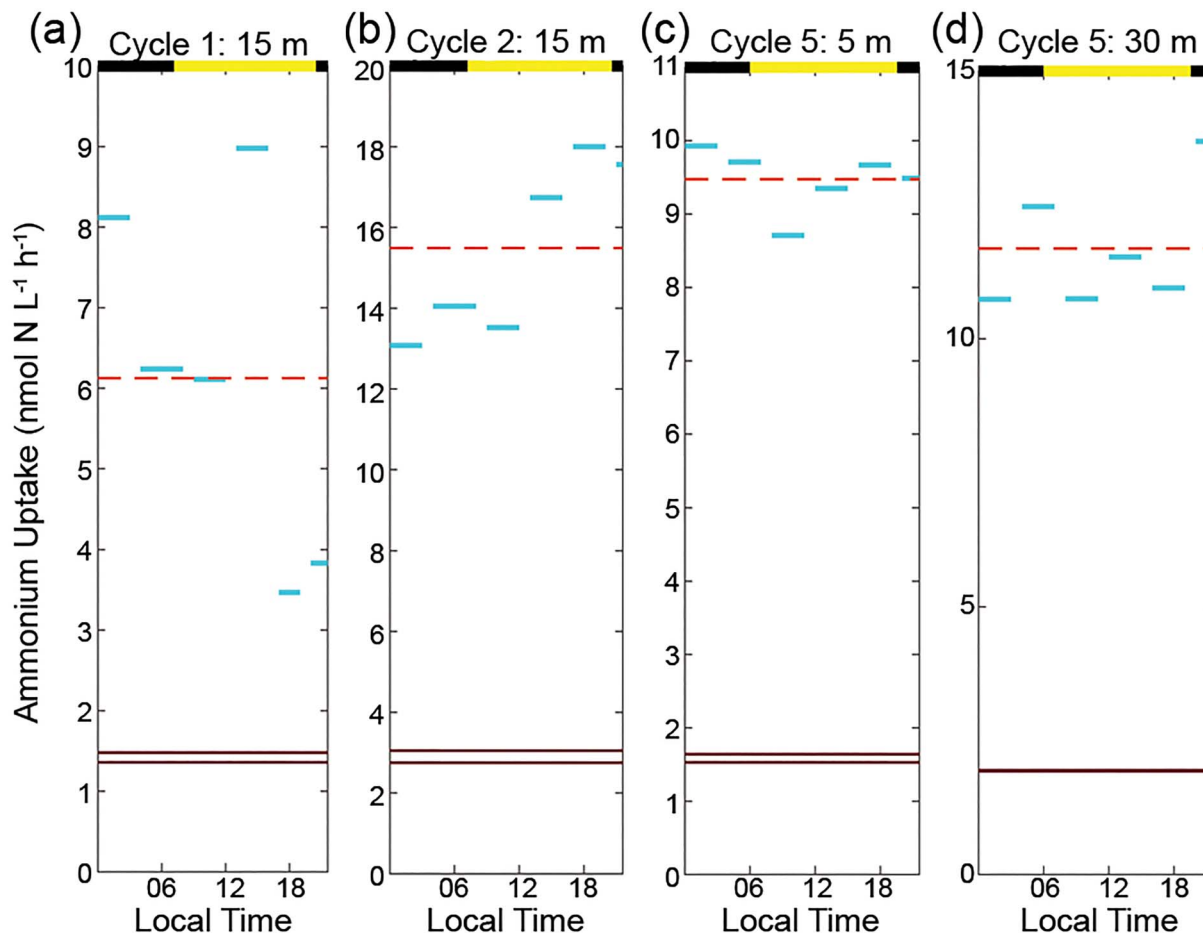


Fig. 3. Diel NH_4^+ uptake rates ($\text{nmol N L}^{-1} \text{h}^{-1}$) with solid horizontal lines showing the duration and mean uptake rates for the 4–5 h (blue) and 24-h (dark brown) incubations. Dashed horizontal lines (orange) represent averages of 4–5 h incubations for comparison with 24-h incubations carried out during the same time frame. Black and yellow alternating bars (top of each figure) represent local daylight and dark hours. Depths indicate depth of water collection and approximate correspondence to incubator light level. Panel (a) represents cycle 1, panel (b) represents cycle 2 and panels (c) and (d) represent cycle 5.

the sums of 4-h incubations were substantially greater than simultaneous 24-h incubations. For NO_3^- uptake, the ratio of the sum of sequential 4-h incubations to the average of 24-h incubations ranged from 1.2 to 5.6 (median = 2.0). For NH_4^+ uptake this ratio ranged from 5.0 to 6.0 (median = 5.7). These results indicate rapid recycling of NH_4^+ in the euphotic zone and also reasonably fast recycling of NO_3^- .

Vertical profiles of phytoplankton growth rates

Instantaneous growth rates of phytoplankton were variable as a function of depth and cycle (Fig. 6). On average, PRO surface growth rates were $0.67 \pm 0.35 \text{ d}^{-1}$, decreasing with depth to $0.27 \pm 0.10 \text{ d}^{-1}$ at the DCM. Similarly, the average SYN surface growth rates were $0.64 \pm 0.29 \text{ d}^{-1}$, decreasing with depth to $0.34 \pm 0.30 \text{ d}^{-1}$

at the DCM. These rates are consistent with previous research (Partensky *et al.*, 1999). DIAT growth, ranging from -0.4 to 1.5 d^{-1} , was higher in the upper euphotic zone and declined gradually with depth, except for a peak at 85 m during C4. ADINO growth ranged from 0 to 1.2 d^{-1} and varied between cruises. In 2017 (C1–C3), growth of ADINOs was highest in the upper mixed layer and gradually declined with depth. In 2018 experiments, (C4–C5), ADINO growth peaked in the mid euphotic zone at $\sim 40 \text{ m}$. PRYM growth rate varied among cycles, ranging from -0.5 to 1.3 d^{-1} with occasional peak values in the mid water column.

Model results

Using a Bayesian statistical approach to assimilate our *in situ* measurements, we constrained typical transfer functions used to model taxon-specific phytoplankton

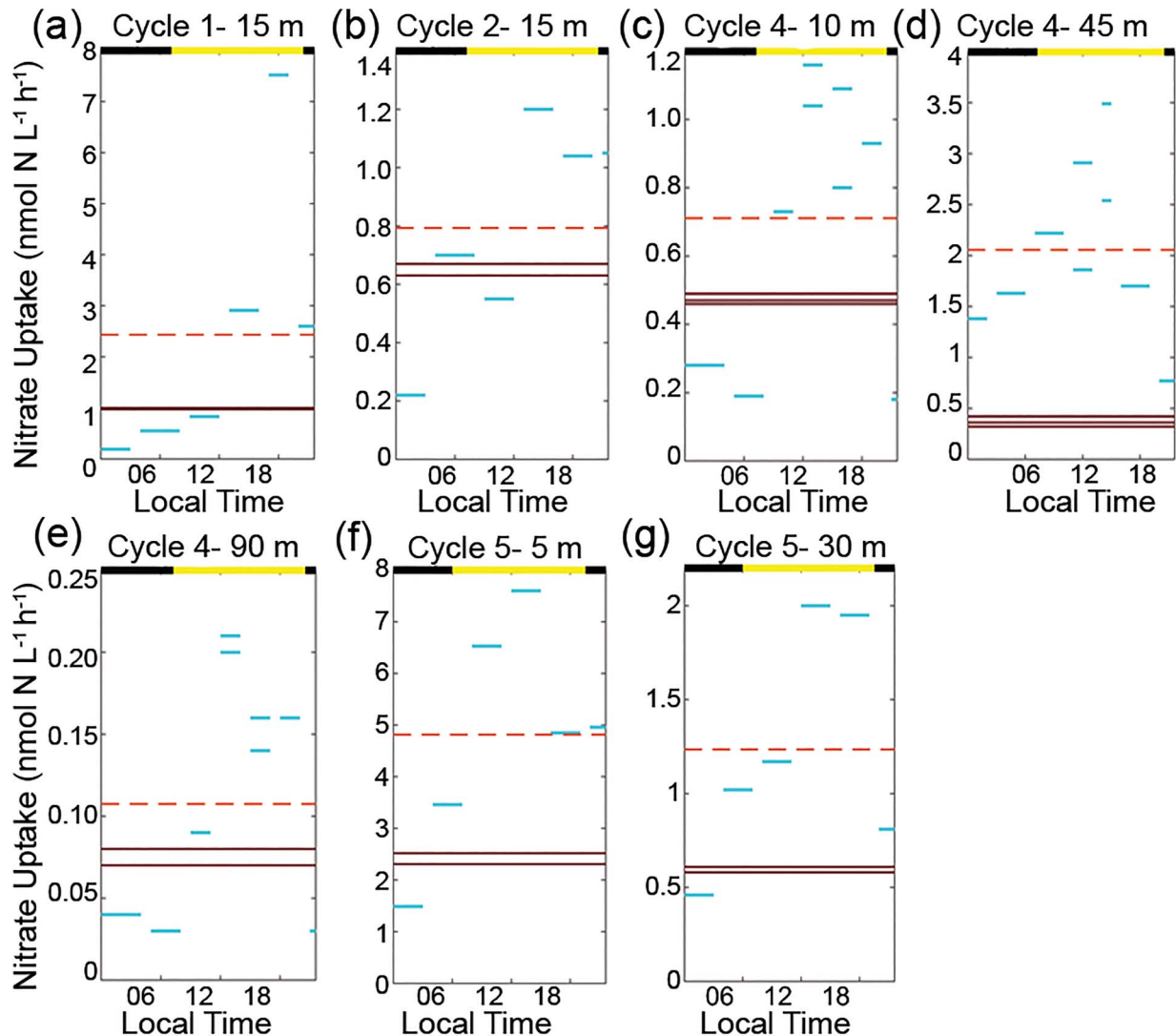


Fig. 4. Diel NO_3^- uptake rates ($\text{nmol N L}^{-1} \text{h}^{-1}$). Depths of water collection for the incubations are indicated next to the cycle number. Solid horizontal lines show the duration and mean uptake rates for the 4–5 h (blue) and 24-h (dark brown) incubations. Dashed horizontal lines (orange) represent averages of 4–5 h incubations for comparison with 24-h incubations carried out during the same time frame. Time periods that had more than one replicate are both shown, e.g. two blue lines at one time period. Black and yellow alternating bars (top of each figure) represent local daylight and dark hours. Panel (a) represents cycle 1; panel (b) represents cycle 2; panels (c), (d) and (e) represent cycle 4 and panels (f) and (g) represent cycle 5.

responses to light, temperature and nutrient limitation in biogeochemical models. Data assimilation increased the fit to experimental data relative to the default parameterization from NEMURO-GoM (Supplemental Fig. S2; Supplemental Table SI). The parameters determined from data assimilation had a much better fit to NPP observations than the default parameters, but only a moderately better fit to nitrate uptake observations (Fig. 7). The assimilated parameters underestimated observed nitrate uptake when nitrate uptake was high (although only by a factor of 2–5, whereas the default parameters underestimated nitrate uptake by ~10-fold).

The model underestimate resulted from the fact that even with low half-saturation constants the NEMURO model did not predict nitrate uptake rates as high as the observations in a region with such low nitrate concentrations. Total model log-likelihood increased substantially after the Bayesian optimization procedure (from -40 748 to -3 333 for NEMURO-GOM default and data-assimilated parameters, respectively, Supplemental Table SI). Notably, the default parameters predicted unrealistically low NPP and growth rates for phytoplankton based on the low nutrient concentrations in the GoM euphotic zone (Supplemental Fig. S2).

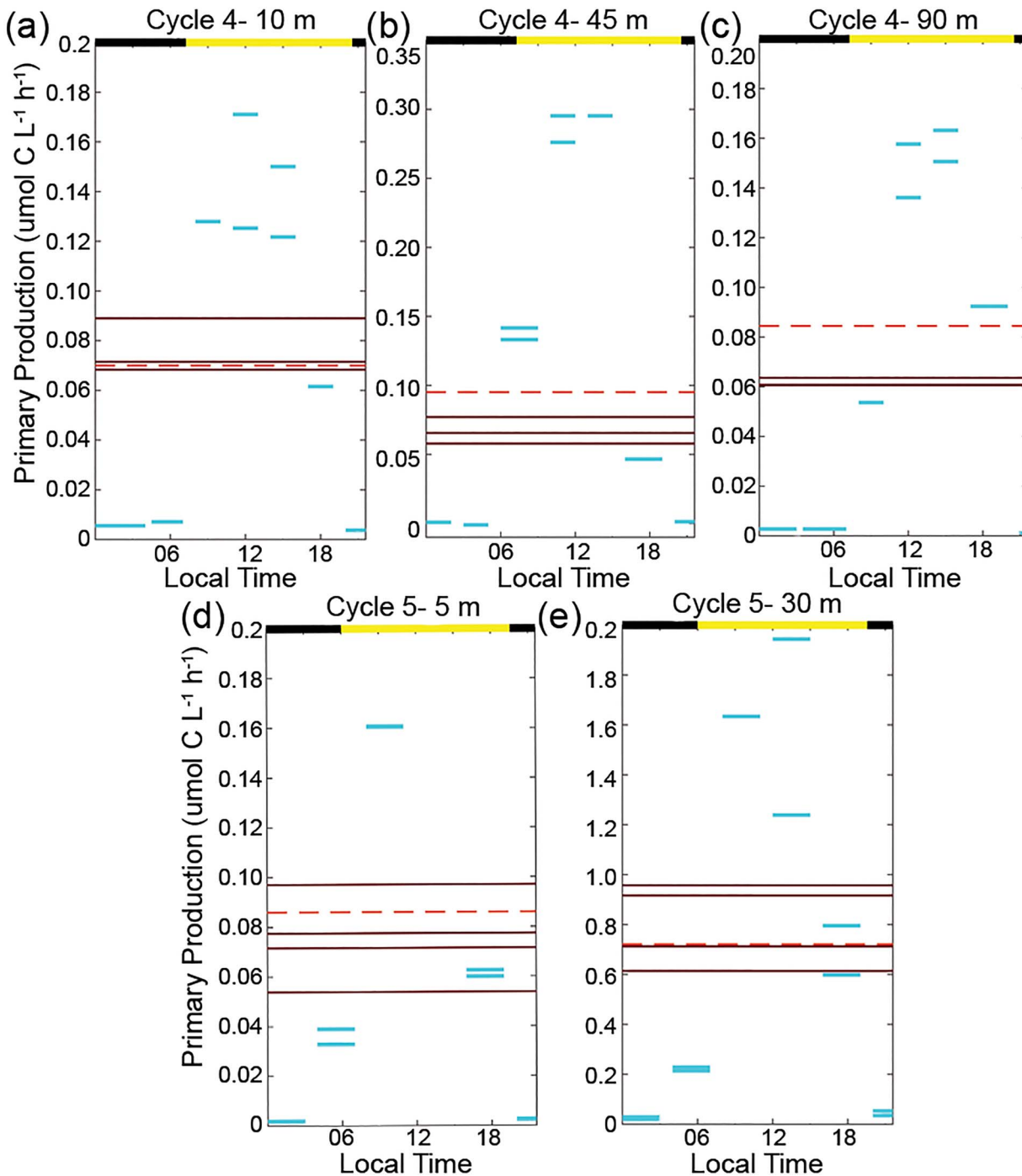


Fig. 5. Diel primary production ($\mu\text{mol C L}^{-1} \text{h}^{-1}$) from shipboard experiments. Solid horizontal lines show the duration and uptake rates for individual 4–5 h (blue) and duplicate 24-h (dark brown) incubations. Time periods that had more than one replicate are both shown, e.g. two blue lines at one time period. Dashed horizontal lines (orange) represent averaged short incubations for comparison with 24-h incubations. Black and yellow bars located at the top of figures represent local daytime and nighttime. Panels (a), (b) and (c) represent cycle 4 and panels (d) and (e) represent cycle 5.

Consequently, the optimized parameter ranges suggested much lower K_{NH_4} (NH_4^+ half-saturation constants) for all phytoplankton taxa except SYN (Fig. 8). K_{NH_4} was lowest

for PRO [mean = $0.007 \mu\text{M}$, 95% confidence interval (CI) = $0.005\text{--}0.009 \mu\text{M}$], which thrives in oligotrophic regions. Previous research supports low half-saturation

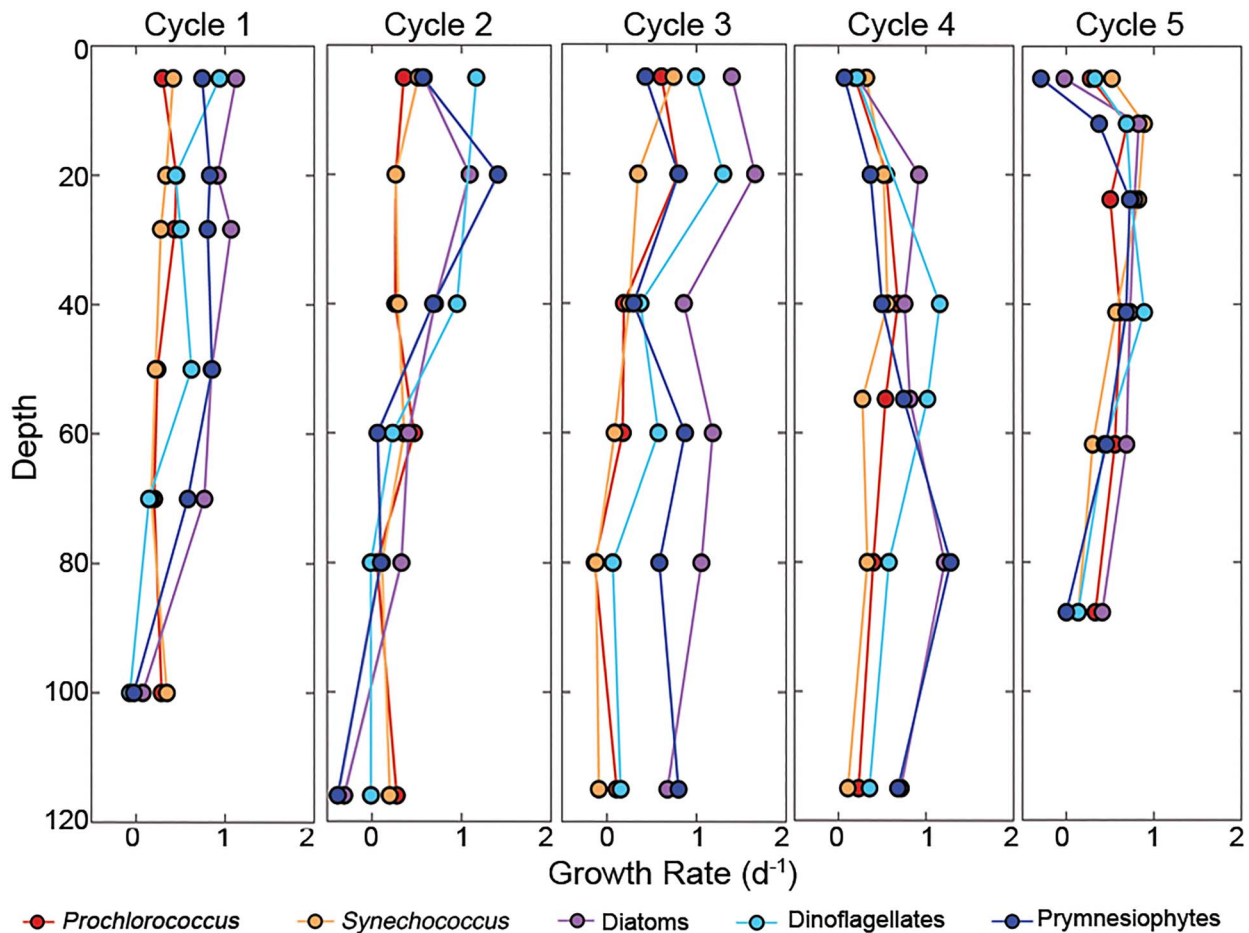


Fig. 6. Dilution experiment results from cycles 1–5, showing averaged group-specific growth rates for *Prochlorococcus*, *Synechococcus*, diatoms, dinoflagellates and prymnesiophytes as a function of depth. Details of experiments are in Landry *et al.*, 2021.

values for PRO (Marañón *et al.*, 2013; Grossowicz *et al.*, 2017). In contrast, the posterior distributions for K_{NO_3} remained relatively close to the prior distributions (and to default NEMURO-GoM parameterizations, Fig. 8). The Bayesian parameter optimization approach suggested K_{NO_3} values of $\sim 3 \mu\text{mol L}^{-1}$ for all large phytoplankton taxa, $\sim 0.4 \mu\text{mol L}^{-1}$ for PRO and OTHER and $\sim 0.1 \mu\text{mol L}^{-1}$ for SYN. This is comparable to laboratory studies that suggest half saturation constants are proportional to cell size with larger cells ranging in value from 0.1 to $5.0 \mu\text{mol L}^{-1}$ (Eppley *et al.*, 1969).

Model results also varied among groups with respect to light-response parameters and maximum growth rates. PRO and OTHER had the lowest maximum growth rates at 25°C ($V_{25^\circ\text{C}} = 0.82 \text{ d}^{-1}$, 95% CI = $0.73\text{--}0.92 \text{ d}^{-1}$; and 0.44 d^{-1} , 95% C.I. = $0.35\text{--}0.54 \text{ d}^{-1}$, respectively, as shown in Supplemental Fig. S2). However, the low maximum growth rate parameter suggested for OTHER might be an artifact of the inclusion of many different taxa within this group, which resulted in the model predicting low

and only weakly varying growth rates. All large phytoplankton taxa had a maximum growth rate at 25°C of $\sim 1.6\text{--}2.0 \text{ d}^{-1}$, whereas SYN had a higher maximum growth rate of $2.6\text{--}4.4 \text{ d}^{-1}$. PRO had the weakest light sensitivity, with α (initial slope of the photosynthesis–irradiance relationship) equal to $0.01 \text{ m}^2 \text{ W}^{-1} \text{ d}^{-1}$ (95%: $0.006\text{--}0.02 \text{ m}^2 \text{ W}^{-1} \text{ d}^{-1}$), which likely reflects the presence of low-light-adapted PRO strains that thrive in the deep euphotic zone. Most taxa had α in the range of $0.02\text{--}0.8 \text{ m}^2 \text{ W}^{-1} \text{ d}^{-1}$ reflecting substantial light limitation and reduced growth rates in the DCM (Fig. 8, Supplemental Fig. S1).

Because we simultaneously varied all parameters, our optimization procedure provides some insight into correlations among parameters. A subset of these results (for PRO) are shown in Fig. 8. For instance, α and V were positively correlated suggesting that the model could fit PRO growth rates at the DCM with either a higher maximum growth rate or with a weaker sensitivity to light limitation. Correlations for PRO were relatively weak for

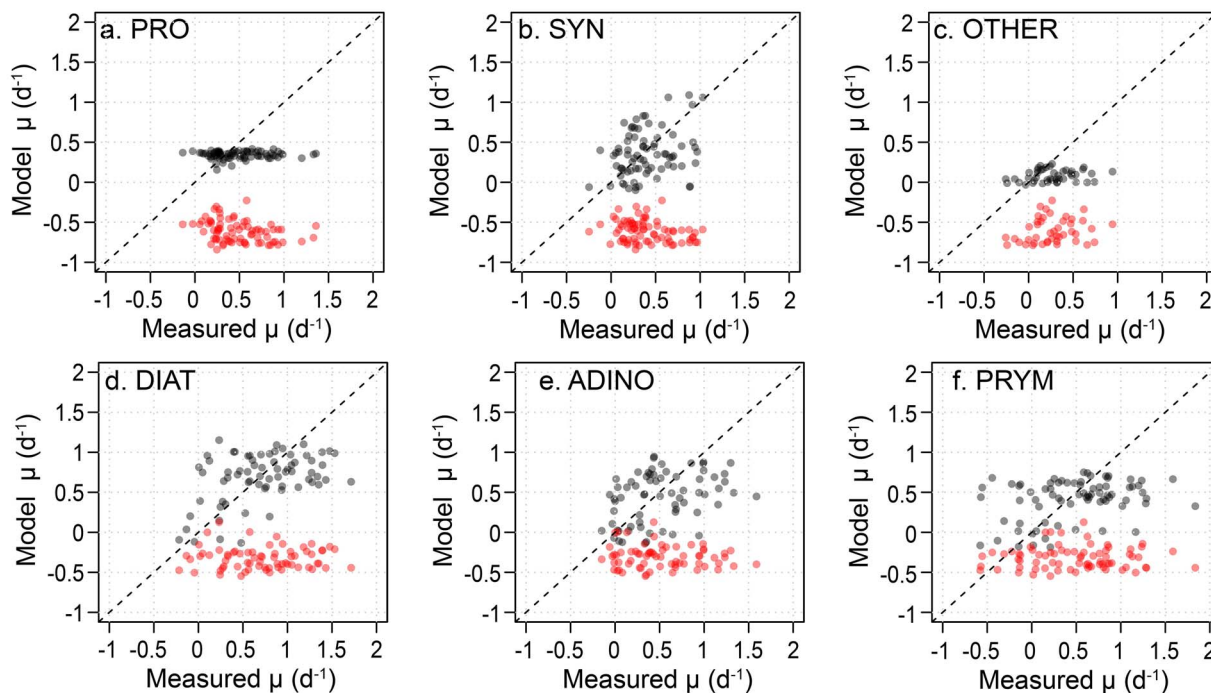


Fig. 7. Model-observation comparisons for (a) NPP and (b) NO_3^- uptake. The dashed line represents the 1:1 ratio. Red dots indicate NEMURO-GoM parameterization while black dots show the “optimized” parameterization. Panel a represents *Prochlorococcus*, panel b represents *Synechococcus*, panel c represents the others group, panel d represents diatoms, panel e represents dinoflagellates, and panel f represents prymnesiophytes.

most parameter pairs. SYN, however, shows strong correlations for several parameter pairs. In particular, nutrient half-saturation constants were positively correlated with each other and with V . This suggests that the model could determine viable solution sets with high maximum growth rates and substantial nutrient limitation or with low maximum growth rates and weaker nutrient limitation and that the relative importance of nutrient limitation by NO_3^- or NH_4^+ could vary (although K_{NO_3} was always lower than K_{NH_4} for SYN).

Comparison of optimized parameter sets with measured environmental conditions (nutrients, light and temperature) also allowed us to assess patterns of limiting resources for each taxon (Fig. 9). While all phytoplankton taxa experienced slightly greater nutrient limitation in the shallow euphotic zone than in the deep euphotic zone, with the exception of SYN, nutrient limitation led to < 50% decrease in growth rates (Fig. 9a). SYN was the only group with a median f -ratio > 0.05. This suggests that all taxa (except SYN) rely disproportionately on ammonium as a N source for growth and primary productivity. In contrast, SYN appeared to be the sole NO_3^- specialist, with commensurately high f -ratios (~ 0.5) and greater nutrient limitation of growth rates. Our model thus shows a distinct niche specialization of the abundant taxa to the oligotrophic nature of this ecosystem.

With the exception of PRO and OTHER, which seem to be well adapted to maintaining low and comparatively insensitive growth rates in both the mixed layer and the deep euphotic zone, all taxa experienced substantial light limitation in the deep euphotic zone (> 50 m). At these depths, light limitation ranged from mild limitation at ~ 50 m depth (e.g. growth penalties of $\sim 20\%$) to strong limitation at the DCM (growth penalties of up to 95%). In comparison, no groups exhibited substantial light limitation above 50 m; the greatest average light limitation penalty in the upper 50 m was for DIAT ($\sim 10\%$), which had the highest photoinhibition parameter.

DISCUSSION

Diel and vertical variability in phytoplankton productivity and nutrient utilization

Our data indicates that the oligotrophic GoM is a highly stratified, picophytoplankton-dominated (mostly PRO) region, with low nitrate concentrations (typically < 0.1 μM above the DCM), low chlorophyll a concentrations (typically < 0.03 $\mu\text{g L}^{-1}$ in the mixed layer and < 0.2 $\mu\text{g L}^{-1}$ in the DCM) and deep DCMs (69–137 m). Nutrient uptake measurements show that

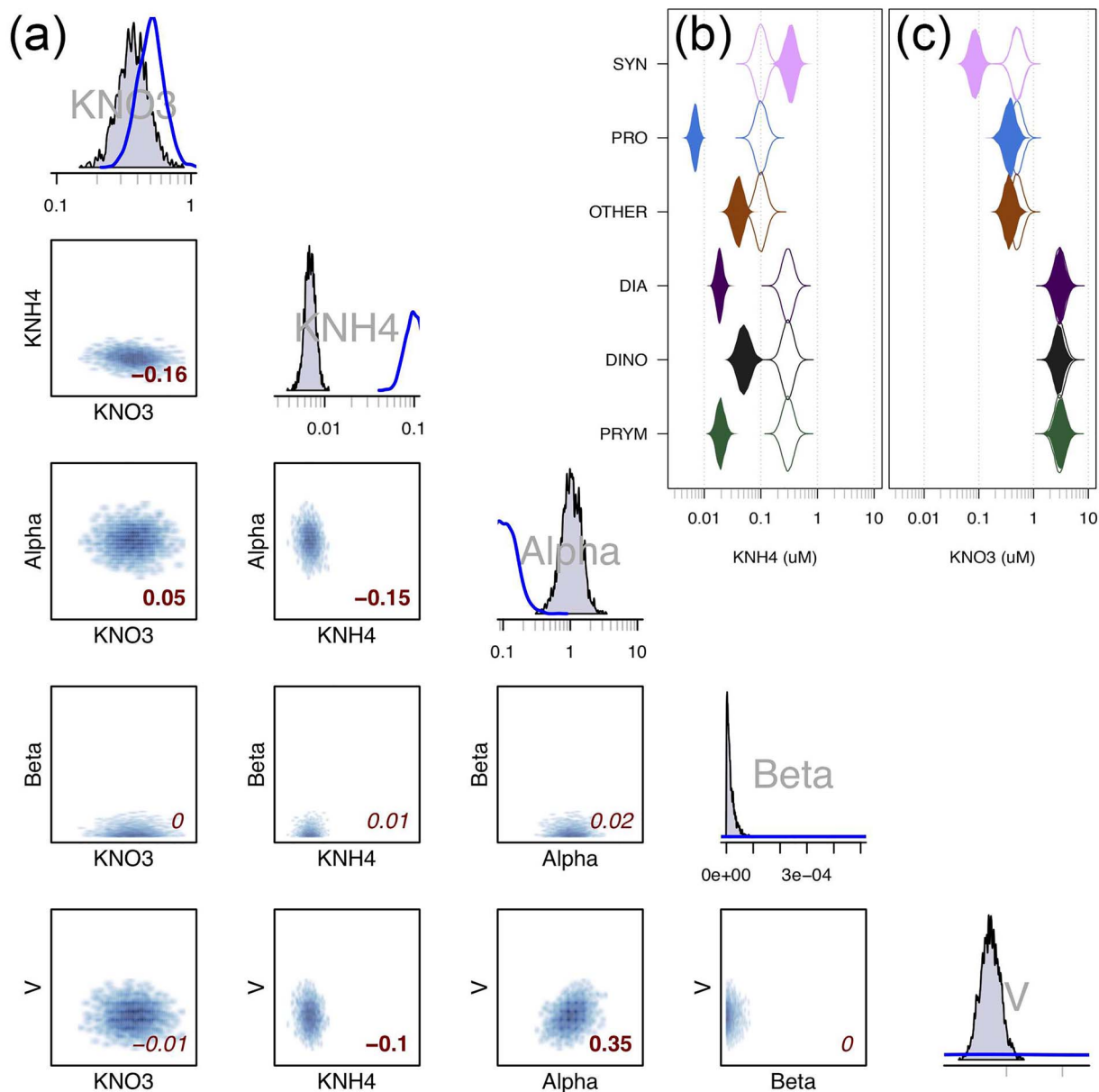


Fig. 8. (a) Model parameters of log-transformed K_{NH_4} ($\mu mol L^{-1}$), log-transformed K_{NO_3} ($\mu mol L^{-1}$), log-transformed α ($m^2 W^{-1} d^{-1}$), β ($m^2 W^{-1} d^{-1}$) and log-transformed V at $0^\circ C$ (d^{-1}) for *Prochlorococcus*. Upper plots are histograms for each variable (filled gray lines, $n = 10^6$, subsampled to 2×10^4), with blue lines approximating the prior distribution that was assumed for each variable from previous studies. Lower property–property plots show the correlation between any two parameters (note that scales are as in the histograms above). Red value located in bottom right corner in each subplot gives Pearson’s correlation coefficient (which is suitable for use with non-normal data, Neftzer and Drasgow, 1957), with bold values indicating significance at $P < 0.05$. Violin plots of (b) NH_4^+ half-saturation constants (K_{NH_4} , μM) and (c) NO_3^- half-saturation constants (K_{NO_3} , μM) from the optimized model (filled) and their priors (empty).

NH_4^+ recycling is key to sustaining the phytoplankton community and productivity. These conclusions are consistent with previous investigations of phytoplankton nutrient limitation in the oceanic GoM (Dugdale and Goering, 1967; Eppley and Peterson, 1979; Platt and Harrison, 1985; Lipschultz, 2001; Wawrik *et al.*, 2004).

Vertical profiles of NPP (Fig. 1) and taxon-specific growth rates (Fig. 6) indicate that phytoplankton and nutrient uptake are generally light limited, with NPP and growth rates declining with depth. This decrease in NPP was not associated with a decline in phytoplankton biomass. Although the biomass of different taxa varied

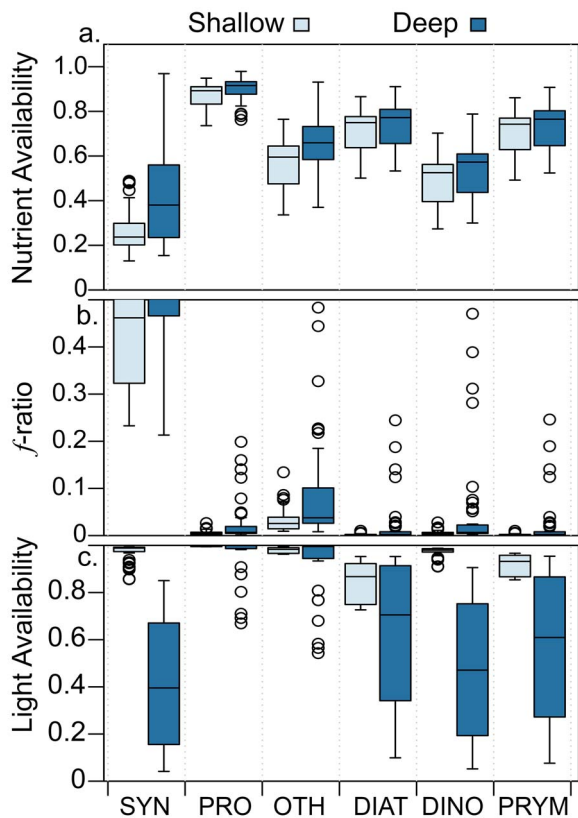


Fig. 9. Modeled results for each phytoplankton group for (a) nitrogen availability (unitless growth rate multiplier equal to $NL + AL$ in equations 1 and 2), (b) f -ratio and (c) light availability (unitless growth rate multiplier equal to LL in equation 3) as a function of depth. Light bars represent shallow water (<math>< 50\text{ m}</math>) and dark bars represent deeper samples (> 50 m). Note that the upper quartile and 95% CI values are offscale for SYN in panel b with values of 0.551 and 0.696 for shallow and 0.699 and 0.921 for deep. See equations 1–4 for formulas and additional information on the calculations.

with depth, overall phytoplankton biomass and particulate organic carbon (POC) were typically relatively constant or increased slightly with depth (Selph *et al.*, 2021; Stukel *et al.*, 2021b). This decrease in productivity and growth is more gradual, however, than might be expected based on light limitation alone. Instead, it reflects substantial nutrient limitation in surface waters that gradually gives way to light limitation in the deeper euphotic zone, suggesting that phytoplankton throughout the euphotic zone grow at rates substantially below their physiological potential. Vertical trends also likely include shifts in species composition. Although these patterns are not evident from our FCM and HPLC-based taxonomic study, sequencing data have shown differentially adapted species within our broad categories, especially for high-light- or low-light-adapted PRO and SYN (Gutiérrez-Rodríguez *et al.*, 2016). Notably, the

distinct DCM was primarily, but not solely, driven by increased cellular pigmentation, as has been seen in multiple other studies (Cullen 1982; Mignot *et al.*, 2014). The maintenance of the DCM despite reduced growth rates thus requires either reduced mortality (i.e. grazing) or subsidies from sinking phytoplankton (Hodges and Rudnick, 2004; Moeller *et al.*, 2019; Stukel *et al.*, 2021b).

The diel experiments showed distinct temporal patterns of NH_4^+ and NO_3^- uptake. NH_4^+ uptake rates did not vary with time of day (Fig. 3), whereas NO_3^- uptake rates were light dependent and similar to diel patterns of NPP (Figs 4 and 5). This is consistent with NO_3^- uptake being more coupled to photosynthetic energy generation while NH_4^+ uptake had no cellular regulation (Figs 3 and 4) (Dortch, 1990). Similar patterns have been found for NO_3^- uptake in the Costa Rica Dome (Stukel *et al.*, 2016). However, NO_3^- uptake rates measured in the Sargasso Sea were lower at night but remained at approximately one-third daytime values (Lipschultz 2001). In the Sargasso Sea, different studies have also given different ratios of daytime to nighttime NH_4^+ uptake, with Lipschultz (2001) determining that daytime rates were twice those of nighttime rates, whereas Glibert *et al.* (1988) found negligible day–night differences (as in our study). Lipschultz (2001) methods included longer incubations (dusk to dawn), whereas Glibert *et al.* (1988) included short 1–2 h incubations. Taken together, these results underline the difficulty in extrapolating from short (2–6-h) experiments to daily uptake rates or f -ratios. Our diel uptake experiments also showed substantial differences between 4 and 24-h NH_4^+ uptake incubations (and to a lesser, but still considerable, extent for NO_3^- uptake incubations). Rapid cycling of NH_4^+ in the surface ocean is expected, while NO_3^- is often considered upwelled “new” nitrogen (Dugdale and Goering, 1967). Recent evidence, however, suggests that NO_3^- regeneration through NH_4^+ oxidation may be more common in surface oceans than previously realized (Yool *et al.*, 2007; Shiozaki *et al.*, 2016). The combination of relatively high rates of NO_3^- uptake (compared with NO_3^- concentration), very low NO_3^- inventory from the surface to the DCM at $\sim 100\text{ m}$ and the ~ 2 -fold higher NO_3^- uptake measured in 4-h incubations relative to 24-h incubations lead us to believe that NO_3^- in the surface GoM might be supplied primarily by NH_4^+ oxidation (Stukel *et al.*, in press).

Model optimization

Accurately constraining biogeochemical model parameters is a challenging yet crucial step toward treating models as falsifiable hypotheses (Arhonditsis and Brett, 2004; Anderson, 2005; Franks, 2009; Schartau *et al.*, 2017). Objective parameterization typically follows two

broad approaches: (i) empirical fits of specific transfer functions to available data or (2) formal data assimilation. The former approach typically fits simple functional forms (e.g. photosynthesis–irradiance curves or Ivlev grazing formulations) to field or laboratory data. Empirical fits can be developed using experimental data derived from intentional manipulation of independent variables for a specific species or community (Eppley *et al.*, 1969; Platt *et al.*, 1980) or determined by fitting relationships for measurements made under natural conditions across an environmental gradient (Li *et al.*, 2010; Morrow *et al.*, 2018). These two empirical approaches address subtly different questions. The former approach examines the mechanistic response of a single taxon to changes in an environmental variable, whereas the latter addresses a similar question but at a community-level scale, thus accounting for community shifts that occur with changes in light and nutrient conditions. This investigation of mechanistic responses at the community level is often more appropriate for models, because most such models simulate plankton functional groups comprised of many different species (Hood *et al.*, 2006). However, it is complicated by frequent covariance of multiple parameters (e.g. light and nutrients).

The alternative approach to model parameterization, which has long been common in physical oceanography, is formal data assimilation (Friedrichs *et al.*, 2006; Gregg *et al.*, 2009; Cummings and Smedstad 2013). In data assimilation, the full forward model is typically run and compared with observations, and then a prescriptive approach is followed to sequentially modify a subset of the parameters to minimize the model-data misfit. While multiple approaches have been used (Lawson *et al.*, 1995; Ward *et al.*, 2010; Doron *et al.*, 2011), the most common approach is the variational adjoint, which is frequently used to compare model outputs with spatial maps of sea surface chlorophyll or time-series measurements of standing stocks in a one-dimensional framework. However, some studies have questioned whether assimilation of standing stock measurements is sufficient to constrain many model parameters or have noted that more complex models often respond less well to assimilation techniques and the tendency of the variational adjoint method to gravitate toward local minima in parameter space (Xiao and Friedrichs, 2014; Löptien and Dietze, 2015).

Our Bayesian statistical approach allows us to simultaneously constrain multiple parameters for which *a priori* estimates contained substantial uncertainty. The incorporation of multiple types of rate measurements allows for more precise determination of posterior distributions than would have been possible if we only utilized standing stock measurements. Indeed, optimized parameter values for the NEMURO-GoM transfer

functions suggest >90% reduction in cost on average (Supplemental Table SI). The results returned reasonable parameter value ranges for most taxa and demonstrated some expected emergent properties (e.g. PRO is an oligotrophic specialist). They also, however, disagreed with *a priori* expectations in some key ways, indicating that likelihood (i.e. our measurements) was more important than prior distributions in determining the posterior distributions. Most notably, the model showed that our experimental results could only be matched using much lower NH_4^+ half-saturation values for most taxa than the default values in NEMURO-GoM or common half-saturation constants measured in cultures (Edwards *et al.*, 2012; Shropshire *et al.*, 2020).

Nevertheless, some parameters seem unrealistic. Notably, the OTHER group, which is a composite of multiple phytoplankton taxa including pelagophytes, chlorophytes, prasinophytes, cryptophytes and other taxa, had very low maximum growth rates (mean: 0.44 d^{-1} , 95%: $0.35\text{--}0.54 \text{ d}^{-1}$ at 25°C) and very little nutrient or light limitation. This suggests that the optimization procedure attempted to give this composite group a low and relatively constant growth rate under all conditions. It is unlikely that pelagophytes, chlorophytes, prasinophytes and cryptophytes were all insensitive to environmental variability. More likely, the different taxa within OTHERS have different responses to light and nutrients that are masked when they are aggregated together in a single group. On the other hand, this aggregate behavior might also be considered a strength of this parameterization approach, since even the most accurate representation of any one taxon or group can never reflect the adaptive physiological potential of a natural mixed community. It is also important to consider that groups like ADINO and OTHERS might be mixotrophic and taking up nitrogen by phagotrophy in this region, which may impact their functional responses to light and nutrient limitation (Jones 2000; Stoecker *et al.*, 2017).

Even though posterior distributions were very different from prior distributions, many of the parameters (e.g. K_{NH_4}) retained substantial uncertainties. These uncertainties arise, in part, from covariance among environmental variables, which leads to correlations across the different parameters. In future work, experimental manipulations could be conducted in ways that break some of the natural correlations (e.g. nutrient amendments or light manipulation). In addition, some uncertainty undoubtedly arises from errors in measurements (nutrients, light, phytoplankton abundance). Future work could explicitly formulate the model such that the inputs are “true” values of standing stocks, defined as $X_i = \hat{X}_i + \delta_{X_i}$ for incubation i , where \hat{X}_i is

the measured value and δ_{X_i} is a random variable with prior distribution centered at 0 and an SD equal to the measurement uncertainty. The δ_{X_i} would then be variables to solve for parameter solutions. Even without these potential improvements, however, we believe that our approach provides useful guidance for parameterizing future biogeochemical models of the GoM and elsewhere.

Phytoplankton niches in the oligotrophic ocean

The vast number of species, strains or ecotypes that are aggregated into our broad phytoplankton taxonomic groups make it difficult to define specific niches for each group (Scanlan, 2003; Simon *et al.*, 2009; Kashtan *et al.*, 2014). It is reasonable to expect that the evolutionary history of taxa provides some inherited physiological constraints on their overall niche space, whereas the prevalence of specific ecotypes may contribute further to a definable niche space for each group. Our results, with respect to both spatial patterns of abundance and model constrained characteristics, shed light on these questions.

The two cyanobacterial taxa have distinctly different ecological niches. For PRO, the consistent subsurface maxima just above the DCM (Selph *et al.*, 2021) and high α (initial slope of the photosynthesis–irradiance curve) indicates that it thrives in low-light conditions. We also observed a substantial increase in divinyl chlorophyll *a* cell⁻¹ with depth that likely explains its physiological adaptation to low light (whether by cellular regulation or distinct ecotypes remains unconstrained). Other studies have shown that there are distinct depth distributions of PRO ecotypes (HLI and HLII near the surface, and LL at low light) (Zwirgmaier *et al.*, 2007). Beyond light limitation, the very low NH₄⁺ half-saturation constant shows it to be a low-nutrient specialist that relies almost exclusively on rapidly recycled NH₄⁺. This concurs with a general consensus that although some strains of PRO contain genes for NO₃⁻ assimilation (Martiny *et al.*, 2009), this genus primarily utilizes NH₄⁺ (Moore *et al.*, 2002). In contrast, SYN was the only group that efficiently exploited low nitrate concentrations, typically maintaining a shallower distribution in the water column with greater sensitivity to light limitation. We thus suspect that SYN relies substantially on NO₃⁻ regenerated in the upper euphotic zone through shallow nitrification (Kelly *et al.*, in review; Stukel *et al.*, in press). Previous research has shown similar fundamental differences between SYN and PRO in nutrient utilization, with SYN utilizing nitrate more efficiently than PRO (Scanlan and West, 2002). Comparisons of abundances to nutrient concentrations and turbulent mixing rates have also suggested that PRO is more abundant in warm waters with low nitrate supply, whereas SYN and picoeukaryote niches are in cooler

waters with greater nitrate supply (Otero-Ferrer *et al.*, 2018), a finding that agrees with previous evidence showing PRO dominance in oligotrophic gyres and SYN and picoeukaryotes becoming more important in equatorial upwelling and temperate regions (Zubkov *et al.*, 2000; Landry and Kirchman, 2002).

Model results for eukaryotic phytoplankton taxa were slightly less conclusive. The larger uncertainty is partially due to the substantially lower abundance of these taxa, and also in part because the pigment-based growth rates were imperfect estimates of true cellular growth of these taxa. DIAT had modest maximum growth rates, lower than those in many culture and field measurements (e.g. Furnas, 1990; Sarthou *et al.*, 2005; Selph *et al.*, 2011; Selph *et al.*, 2016). This might, however, reflect chronic extreme silicon limitation, which was not assessed in our study. We do note that prior concentration measurements from GoM indicate that Si is very low (Dortch and Whitlege, 1992). Irwin *et al.* (2012) used continuous-plankton-recorder-derived phytoplankton abundance data to show that diatoms and dinoflagellates have distinct ecological niches with diatoms typically excelling in cold, nutrient-rich, well-mixed, low-light environments relative to dinoflagellates, which agrees with the low diatom biomasses we found. Barton *et al.* (2015) further showed that diatom responses to these physical drivers are spatiotemporally variable, which does suggest caution when applying our results to other regions. Our model could not significantly differentiate between ADINO and PRYMN, both of which had maximum growth rates of ~ 0.6 d⁻¹ and exhibited substantial light limitation. The model did, however, suggest that the NH₄⁺ half-saturation constant was substantially lower for PRYMN than ADINO, which is not surprising for a generally smaller phytoplankton taxon and might help explain why PRYM was the biomass-dominant eukaryote in our study (Selph *et al.*, 2021). Considered together, these results delineate distinct competitive differences between these diverse phytoplankton functional groups, which help explain their coexistence in oligotrophic conditions and support the advanced light and nutrient resource competition model (Burson *et al.* 2018).

CONCLUSION

The oceanic GoM is an extremely oligotrophic ecosystem with low NPP and a strong DCM. We found higher NPP in the upper euphotic zone than the DCM, fueled mostly by recycled nutrients. Ammonium uptake exceeded nitrate uptake at all depths and was relatively invariant with time of day, whereas nitrate uptake was mainly restricted to daytime. Bayesian parameter optimization techniques allowed us to constrain maximum growth

rates, light utilization parameters and half saturation constants for five phytoplankton taxa (PRO, SYN, DIAT, PRYMN and ADINO), yielding parameter values for future modeling studies. This approach also allowed us to define distinct niches for different taxa and determine that all, except PRO, were chronically nutrient limited at all depths.

SUPPLEMENTARY DATA

Supplementary data is available at *Journal of Plankton Research* online.

ACKNOWLEDGEMENTS

This manuscript would not have been possible without the support from the captain, crew and research technicians aboard the NOAA Ship “Nancy Foster”; thank you for your dedication and hard work. In addition, we would like to acknowledge and thank our collaborators at NOAA Southeast Fisheries/RAS-MAS/University of Miami for their effort and perseverance on leading two successful cruises.

FUNDING

BLOOFINZ-GoM Program support from the National Oceanic and Atmospheric Administration’s RESTORE Program Grant (Project Title: Effects of nitrogen sources and plankton food-web dynamics on habitat quality for the larvae of Atlantic bluefin tuna in the Gulf of Mexico) under federal funding opportunity NOAA-NOS-NCCOS-2017-2004875, including NOAA JIMAR Cooperative Agreement, award #NA16NMF4320058, NOAA CIMAS Cooperative Agreement, award #NA15OAR4320064 and NOAA CIMEAS Cooperative Agreement, award #NA15OAR4320071.

DATA ARCHIVING

Data presented here have been submitted to the National Oceanic and Atmospheric Administration’s (NOAA) National Centers for Environmental Information (NCEI) data repository and will also be archived at BCO-DMO (Biological and Chemical Oceanography Data Management Office) site <https://www.bco-dmo.org/program/819631>. Model code and dataset are freely available on Github (<https://github.com/tbrycekelly/Yingling/>) with instructions on how to replicate model results.

REFERENCES

Anderson, T. R. (2005) Plankton functional type modelling: running before we can walk? *J. Plankton Res.*, **27**, 1073–1081.

Arhonditsis, G. B. and Brett, M. T. (2004) Evaluation of the current state of mechanistic aquatic biogeochemical modeling. *Mar. Ecol. Prog. Ser.*, **271**, 13–26.

Barton, A. D., Lozier, M. S. and Williams, R. G. (2015) Physical controls of variability in North Atlantic phytoplankton communities. *Limnol. Oceanogr.*, **60**, 181–197.

Biggs, D. C. (1992) Nutrients, plankton, and productivity in a warm-core ring in the western Gulf of Mexico. *J. Geophys. Res: Oceans.*, **97**, 2143–2154.

Biggs, D. C., Hu, C. and Müller-Karger, F. E. (2008) Remotely sensed sea-surface chlorophyll and POC flux at Deep Gulf of Mexico Benthos sampling stations. *Deep-Sea Res. II*, **55**, 2555–2562.

Biggs, D. C. and Ressler, P. H. (2001) Distribution and abundance of phytoplankton, zooplankton, ichthyoplankton, and micronekton in the deepwater Gulf of Mexico. *Gulf of Mex. Sci.*, **19**, 1–23.

Burson, A., Stomp, M., Greenwell, E., Grosse, J. and Huisman, J. (2018) Competition for nutrients and light: testing advances in resource competition with a natural phytoplankton community. *Ecology*, **99**, 1108–1118.

Chisholm, S. W., Olson, R. J., Zettler, E. R., Goericke, R., Waterbury, J. B. and Welschmeyer, N. A. (1988) A novel free-living prochlorophyte abundant in the oceanic euphotic zone. *Nature*, **334**, 340–343.

Cornic, M., Smith, B. L., Kitchens, L. L., Bremer, J. R. A. and Rooker, J. R. (2018) Abundance and habitat associations of tuna larvae in the surface water of the Gulf of Mexico. *Hydrobiologia*, **806**, 29–46.

Cullen, J. J. (1982) The deep chlorophyll maximum: comparing vertical profiles of chlorophyll a. *Can. J. Fish. Aquat. Sci.*, **39**, 791–803.

Cummings, J. A. and Smedstad, O. M. (2013) Variational data assimilation for the global ocean. In *Data Assimilation for Atmospheric, Oceanic and Hydrologic Applications*, Springer, Berlin, Heidelberg, pp. 303–343.

Davey, M., Tarran, G. A., Mills, M. M., Ridame, C., Geider, R. J. and Laroche, J. (2008) Nutrient limitation of picophytoplankton photosynthesis and growth in the tropical North Atlantic. *Limnol. Oceanogr.*, **53**, 1722–1733.

De Martini, F., Neuer, S., Hamill, D., Robidart, J. and Lomas, M. W. (2018) Clade and strain specific contributions of *Synechococcus* and *Prochlorococcus* to carbon export in the Sargasso Sea. *Limnol. Oceanogr.*, **63**, 448–457.

Doron, M., Brasseur, P. and Brankart, J. M. (2011) Stochastic estimation of biogeochemical parameters of a 3D ocean coupled physical-biogeochemical model: twin experiments. *J. Mar. Syst.*, **87**, 194–207.

Dortch, Q. (1990) The interaction between ammonium and nitrate uptake in phytoplankton. *Mar. Ecol. Prog. Ser.*, **61**, 183–201.

Dortch, Q. and Whittedge, T. E. (1992) Does nitrogen or silicon limit phytoplankton production in the Mississippi River plume and nearby regions? *Cont. Shelf Res.*, **12**, 1293–1309.

Duce, R. A., LaRoche, J., Altieri, K., Arrigo, K. R., Baker, A. R., Capone, D. G., Cornell, S., Dentener, F. *et al.* (2008) Impacts of atmospheric anthropogenic nitrogen on the open ocean. *Science*, **320**, 893–897.

Dugdale, R. C. and Goering, J. J. (1967) Uptake of new and regenerated forms of nitrogen in primary productivity. *Limnol. Oceanogr.*, **12**, 196–206.

Dugdale, R. C. and Wilkerson, F. P. (1986) The use of 15N to measure nitrogen uptake in eutrophic: experimental considerations. *Limnol. Oceanogr.*, **31**, 673–689.

Dutkiewicz, S., Scott, J. R. and Follows, M. J. (2013) Winners and losers: ecological and biogeochemical changes in a warming ocean. *Global Biogeochem. Cycles*, **27**, 463–477.

Edwards, K. F., Thomas, M. K., Klausmeier, C. A. and Litchman, E. (2012) Allometric scaling and taxonomic variation in nutrient utilization traits and maximum growth rate of phytoplankton. *Limnol. Oceanogr.*, **57**, 554–566.

- Eppley, R. W. and Peterson, B. J. (1979) Particulate organic matter flux and planktonic new production in the deep ocean. *Nature*, **282**, 677–680.
- Eppley, R. W., Rogers, J. N. and McCarthy, J. J. (1969) Half-saturation constants for uptake of nitrate and ammonium by marine phytoplankton. *Limnol. Oceanogr.*, **14**, 912–920.
- Follows, M. J. and Dutkiewicz, S. (2011) Modeling diverse communities of marine microbes. *Ann. Rev. Mar. Sci.*, **3**, 427–451.
- Forristall, G. Z., Schaudt, K. J. and Cooper, C. K. (1992) Evolution and kinematics of a loop current eddy in the Gulf of Mexico during 1985. *J. Geophys. Res.: Oceans*, **97**, 2173–2184.
- Franks, P. J. (2009) Planktonic ecosystem models: perplexing parameterizations and a failure to fail. *J. Plankton Res.*, **31**, 1299–1306.
- Friedrichs, M. A. M., Hood, R. R. and Wiggert, J. D. (2006) Ecosystem model complexity versus physical forcing: quantification of their relative impact with assimilated Arabian Sea data. *Deep-Sea Res. II*, **53**, 576–600.
- Furnas, M. J. (1990) *In situ* growth rates of marine phytoplankton: approaches to measurement, community and species growth rates. *J. Plankton Res.*, **12**, 1117–1151.
- Gerard, T., Lamkin, J. T., Kelly, T. B., Knapp, A. N., Laiz-Carrión, R., Malca, E., Selph, K. E., Shiroza, A. *et al.* (2021) Bluefin larvae in Oligotrophic Ocean foodwebs, investigations of nutrients to zooplankton: overview of the BLOOFINZ-Gulf of Mexico program. *J. Plankton Res.*
- Glibert, P. M., Dennett, M. R. and Caron, D. A. (1988) Nitrogen uptake and NH₄⁺ regeneration by pelagic microplankton and marine snow from the North Atlantic. *J. Mar. Res.*, **46**, 837–852.
- Gomez, F. A., Lee, S.-K., Liu, Y., Hernandez, F. J. Jr., Müller-Karger, F. E. and Lamkin, J. T. (2018) Seasonal patterns in phytoplankton biomass across the northern and deep Gulf of Mexico: a numerical model study. *Biogeo.*, **15**, 3561–3576.
- Gregg, W. W., Friedrichs, M. A., Robinson, A. R., Rose, K. A., Schlitzer, R., Thompson, K. R. and Doney, S. C. (2009) Skill assessment in ocean biological data assimilation. *J. Mar. Syst.*, **76**, 16–33.
- Grossowicz, M., Roth-Rosenberg, D., Aharonovich, D., Silverman, J., Follows, M. J. and Sher, D. (2017) *Prochlorococcus* in the lab and *in silico*: the importance of representing exudation. *Limnol. Oceanogr.*, **62**, 818–835.
- Gutiérrez-Rodríguez, A., Selph, K. E. and Landry, M. R. (2016) Phytoplankton growth and microzooplankton grazing dynamics across vertical environmental gradients determined by transplant *in situ* dilution experiments. *J. Plankton Res.*, **38**, 271–289.
- Hastings, W. K. (1970) Monte Carlo sampling methods using Markov chains and their applications. *Biometrika*, **57**, 97–109.
- Higgins, H., Wright, S. and Schlüter, L. (2011) Quantitative interpretation of chemotaxonomic pigment data. In Roy, S., Llewellyn, C., Ege-land, E. and Johnsen, G. (eds.), *Phytoplankton Pigments: Characterization, Chemotaxonomy and Applications in Oceanography*, Cambridge University Press, Cambridge, pp. 257–313.
- Hodges, B. A. and Rudnick, D. L. (2004) Simple models of steady deep maxima in chlorophyll and biomass. *Deep Sea Res. I*, **51**, 999–1015.
- Hood, R. R., Laws, E. A., Armstrong, R. A., Bates, N. R., Brown, C. W., Carlson, C. A., Chai, F., Doney, S. C. *et al.* (2006) Pelagic functional group modeling: progress, challenges and prospects. *Deep-Sea Res. II*, **53**, 459–512.
- Irwin, A. J., Nelles, A. M. and Finkel, Z. V. (2012) Phytoplankton niches estimated from field data. *Limnol. Oceanogr.*, **57**, 787–797.
- Jones, R. I. (2000) Mixotrophy in planktonic protists: an overview. *Freshwater Biol.*, **45**, 219–226.
- Kashtan, N., Roggensack, S. E., Rodrigue, S., Thompson, J. W., Biller, S. J., Coe, A., Ding, H., Marttinen, P. *et al.* (2014) Single-cell genomics reveals hundreds of coexisting subpopulations in wild *Prochlorococcus*. *Science*, **344**, 416–420.
- Kelly, T. B., Knapp, A. N., Landry, M. R., Selph, K. E., Shropshire, T. A., Thomas, R. and Stukel, M. R. Lateral advection supports nitrogen export in the oligotrophic open-ocean Gulf of Mexico. *Nat. Comm.*, in review.
- Kent, A. G., Dupont, C. L., Yooseph, S. and Martiny, A. C. (2016) Global biogeography of *Prochlorococcus* genome diversity in the surface ocean. *ISME J.*, **10**, 1856–1865.
- Knapp, A. N., Thomas, R., Stukel, M. R., Kelly, T. B., Landry, M. R., Selph, K. E., Malca, E., Gerard, T. *et al.* (2021) Constraining the sources of nitrogen fueling export production in the Gulf of Mexico using nitrogen isotope budgets. *J. Plankton Res.*
- Landry, M. R., Brown, S. L., Rii, Y. M., Selph, K. E., Bidigare, R. R., Yang, E. J. and Simmons, M. P. (2008) Depth-stratified phytoplankton dynamics in Cyclone *Opal*, a subtropical mesoscale eddy. *Deep-Sea Res. II*, **55**, 1348–1359.
- Landry, M. R. and Hassett, R. P. (1982) Estimating the grazing impact of marine microzooplankton. *Mar. Biol.*, **67**, 283–288.
- Landry, M. R. and Kirchman, D. L. (2002) Microbial community structure and variability in the tropical Pacific. *Deep-Sea Res. II*, **49**, 2669–2694.
- Landry, M. R., Ohman, M. D., Goericke, R., Stukel, M. R. and Tsyrlkevich, K. (2009) Lagrangian studies of phytoplankton growth and grazing relationships in a coastal upwelling ecosystem off Southern California. *Prog. Oceanogr.*, **83**, 208–216.
- Landry, M. R., Selph, K. E., Stukel, M. R., Swalethorp, R., Kelly, T. B., Beatty, J. and Quackenbush, C. (2021) Microbial food web dynamics in the oceanic Gulf of Mexico. *J. Plankton Res.* doi: 10.1093/plankt/fbab021.
- Landry, M. R., Selph, K. E. and Yang, E.-J. (2011) Decoupled phytoplankton growth and microzooplankton grazing in the deep euphotic zone of the HNLC equatorial Pacific. *Mar. Ecol. Prog. Ser.*, **421**, 13–24.
- Lawson, L. M., Spitz, Y. H., Hofmann, E. E. and Long, R. B. (1995) A data assimilation technique applied to a predator-prey model. *Bull. Math. Biol.*, **57**, 593–617.
- Li, Q. P., Franks, P. J., Landry, M. R., Goericke, R. and Taylor, A. G. (2010) Modeling phytoplankton growth rates and chlorophyll to carbon ratios in California coastal and pelagic ecosystems. *Eur. J. Vasc. Endovasc. Surg.*, **115**, 1–12.
- Li, J., Plouchart, D., Zastepa, A. and Dittrich, M. (2019) Picoplankton accumulate and recycle polyphosphate to support high primary productivity in coastal Lake Ontario. *Sci. Rep.*, **9**, 1–10.
- Lipschultz, F. (2001) A time-series assessment of the nitrogen cycle at BATS. *Deep-Sea Res. II*, **48**, 1897–1924.
- Löptien, U. and Dietze, H. (2015) Constraining parameters in marine pelagic ecosystem models—is it actually feasible with typical observations of standing stocks? *Ocean Sci.*, **11**, 573–590.
- Marañón, E., Cermeño, P., López-Sandoval, D. C., Rodríguez-Ramos, T., Sobrino, C., Huete-Ortega, M., Blanco, J. M. and Rodríguez, J. (2013) Unimodal size scaling of phytoplankton growth and the size dependence of nutrient uptake and use. *Eco. Lett.*, **16**, 371–379.
- Martiny, A. C., Kathuria, S. and Berube, P. M. (2009) Widespread metabolic potential for nitrite and nitrate assimilation among *Prochlorococcus* ecotypes. *Proc. Natl. Acad. Sci.*, **106**, 10787–10792.

- Mignot, A., Claustre, H., Uitz, J., Poteau, A., d'Ortenzio, F. and Xing, X. (2014) Understanding the seasonal dynamics of phytoplankton biomass and the deep chlorophyll maximum in oligotrophic environments: a Bio-Argo float investigation. *Global Biogeochem. Cycles*, **28**, 856–876.
- Moeller, H. V., Laufkötter, C., Sweeney, E. M. and Johnson, M. D. (2019) Light-dependent grazing can drive formation and deepening of deep chlorophyll maxima. *Nat. Commun.*, **10**, 1–8.
- Monterey, G. and Levitus, S. (1997) *Seasonal Variability of Mixed Layer Depths for the World, NOAA Atlas NESDIS 14*, US Government Printing Office, Washington, DC.
- Moore, L. R., Post, A. F., Rocap, G. and Chisholm, S. W. (2002) Utilization of different nitrogen sources by the marine cyanobacteria *Prochlorococcus* and *Synechococcus*. *Limnol. Oceanogr.*, **47**, 989–996.
- Morrow, R., Goericke, R., Kelly, T. B., Landry, M. R., Ohman, M. D., Stephens, B. M. and Stukel, M. R. (2018) Primary productivity, mesozooplankton grazing, and the biological pump in the California current ecosystem: variability and response to El Niño. *Deep-Sea Res. I*, **140**, 52–62.
- Mulholland, M. R., Bernhardt, P. W., Heil, C. A., Bronk, D. A. and O'Neil, J. M. (2006) Nitrogen fixation and release of fixed nitrogen by *Trichodesmium* spp. in the Gulf of Mexico. *Limnol. Oceanogr.*, **51**, 1762–1776.
- Mulholland, M. R. and Lomas, M. W. (2008) Chapter 7: nitrogen uptake and assimilation. *Nitrogen in the marine environment*, 2nd edn. Academic Press, San Diego, pp 303–384.
- Nefzger, M. D. and Drasgow, J. (1957) The needless assumption of normality in Pearson's *r*. *Am. Psychol.*, **12**, 623–625.
- Otero-Ferrer, J. L., Cermeño, P., Bode, A., Fernández-Castro, B., Gasol, J. M., Morán, X. A. G., Marañón, E., Moreira-Coello, V. *et al.* (2018) Factors controlling the community structure of picoplankton in contrasting marine environments. *Biogeosciences*, **15**, 1699–6220.
- Oey, L., Ezer, T. and Lee, H. (2005) Loop current, rings and related circulation in the Gulf of Mexico: a review of numerical models and future challenges. *Geo. Monogr. Am. Geo. Union*, **161**, 31.
- Partensky, F., Hess, W. R. and Vaulot, D. (1999) *Prochlorococcus*, a marine photosynthetic prokaryote of global significance. *Microbiol. Mol. Biol. Rev.*, **63**, 106–127.
- Platt, T. G. C. L., Gallegos, C. L. and Harrison, W. G. (1980) Photoinhibition of photosynthesis in natural assemblages of marine phytoplankton. *J. Mar. Res.*, **38**, 687–701.
- Platt, T. and Harrison, W. G. (1985) Biogenic fluxes of carbon and oxygen in the ocean. *Nature*, **318**, 55–58.
- Redfield, A. C., Ketchum, B. H. and Richards, F. A. (1963) The influence of organisms on the composition of sea water. In Hill, M. N., Ed., *The Sea*, Vol. **2**, Interscience Publishers, New York, 26–77.
- Rooker, J. R., Bremer, J. R. A., Block, B. A., Dewar, H., De Metrio, G., Corriero, A., Kraus, R. T., Prince *et al.* (2007) Life history and stock structure of Atlantic bluefin tuna (*Thunnus thynnus*). *Rev. Fish. Sci.*, **15**, 265–310.
- Sarthou, G., Timmermans, K. R., Blain, S. and Tréguer, P. (2005) Growth physiology and fate of diatoms in the ocean: a review. *J. Sea Res.*, **53**, 25–42.
- Scanlan, D. J. (2003) Physiological diversity and niche adaptation in marine *Synechococcus*. *Adv. Microb. Physiol.*, **47**, 1–64.
- Scanlan, D. J. and West, N. J. (2002) Molecular ecology of the marine cyanobacterial genera *Prochlorococcus* and *Synechococcus*. *FEMS Microbiol. Ecol.*, **40**, 1–12.
- Schartau, M., Wallhead, P., Hemmings, J., Löptien, U., Kriest, I., Krishna, S., Ward, B. A., Slawig, T. *et al.* (2017) Reviews and syntheses: parameter identification in marine planktonic ecosystem modelling. *Biogeosciences*, **14**, 1647–1701.
- Selph, K. E., Landry, M. R., Taylor, A. G., Gutierrez-Rodriguez, A., Stukel, M. R., Wokuluk, J. and Pasulka, A. (2016) Phytoplankton production and taxon-specific growth rates in the Costa Rica Dome. *J. Plankton Res.*, **38**, 199–215.
- Selph, K. E., Landry, M. R., Taylor, A. G., Yang, E. J., Measures, C. I., Yang, J., Stukel, M. R., Christensen, S. *et al.* (2011) Spatially-resolved taxon-specific phytoplankton production and grazing dynamics in relation to iron distributions in the Equatorial Pacific between 110 and 140°W. *Deep-Sea Res. II*, **58**, 358–377.
- Selph, K. E., Swalethorp, R., Stukel, M. R., Kelly, T. B., Knapp, A. N., Fleming, K., Hernandez, T. and Landry, M. R. (2021) Phytoplankton community composition and biomass in the oligotrophic Gulf of Mexico. *J. Plankton Res.* doi: [10.1093/plankt/fbab006](https://doi.org/10.1093/plankt/fbab006).
- Shiozaki, T., Ijichi, M., Isobe, K., Hashihama, F., Nakamura, K. I., Ehama, M., Hayashizaki, K., Takahashi, K. *et al.* (2016) Nitrification and its influence on biogeochemical cycles from the equatorial Pacific to the Arctic Ocean. *ISME J.*, **10**, 2184–2197.
- Shropshire, T. A., Morey, S. L., Chassignet, E. P., Bozec, A., Coles, V. J., Landry, M. R., Swalethorp, R., Zapfe, G. *et al.* (2020) Quantifying spatiotemporal variability in zooplankton dynamics in the Gulf of Mexico with a physical-biogeochemical model. *Biogeosciences*, **17**, 3385–3407.
- Shropshire, T. A., Morey, S. L., Chassignet, E. P., Karnauskas, M., Coles, V. J., Malca, E., Laiz-Carrión, R., Fiksen, O. *et al.* (2021) Trade-offs between risks of predation and starvation in larvae make the shelf break an optimal spawning location for Atlantic Bluefin tuna. *J. Plankton Res.*
- Simon, N., Cras, A. L., Foulon, E. and Lemee, R. (2009) Diversity and evolution of marine phytoplankton. *C. R. Biol.*, **332**, 159–170.
- Stoecker, D. K., Hansen, P. J., Caron, D. A. and Mitra, A. (2017) Mixotrophy in the marine plankton. *Ann. Rev. Mar. Sci.*, **9**, 311–335.
- Strickland, J. D. H. and Parsons, T. R. (1972) A practical handbook of seawater analysis. *Bull. Fish. Res. Board Can.*, **167**, 1–130.
- Stukel, M. R. (2020) Investigating equations for measuring dissolved inorganic nutrient uptake in oligotrophic conditions. *bioRxiv*, 2020.08.30.274449.
- Stukel, M. R., Benitez-Nelson, C. R., Decima, M., Taylor, A. G., Buchwald, C. and Landry, M. R. (2016) The biological pump in the Costa Rica Dome: an open-ocean upwelling system with high new production and low export. *J. Plankton Res.*, **38**, 348–365.
- Stukel, M. R., Gerard, T., Kelly, T. B., Knapp, A. N., Laiz-Carrión, R., Lamkin, J. T., Landry, M. R., Malca, E. *et al.* (in press) Plankton food webs in the oligotrophic Gulf of Mexico spawning ground of Atlantic bluefin. *J. Plankton Res.* doi: [10.1093/plankt/fbab023](https://doi.org/10.1093/plankt/fbab023).
- Stukel, M. R., Kelly, T. B., Landry, M. R., Selph, K. E. and Swalethorp, R. (2021b) Sinking carbon, nitrogen, and pigment flux within and beneath the euphotic zone in the oligotrophic, open-ocean Gulf of Mexico. *J. Plankton Res.* doi: [10.1093/plankt/fbab001](https://doi.org/10.1093/plankt/fbab001).
- Stukel, M. R., Kahru, M., Benitez-Nelson, C. R., Decima, M., Goericke, R., Landry, M. R. and Ohman, M. D. (2015) Using Lagrangian-based process studies to test satellite algorithms of vertical carbon flux in the eastern North Pacific Ocean. *J. Geophys. Res.: Oceans*, **120**, 7208–7222.

- Walker, N. D., Leben, R. R. and Balasubramanian, S. (2005) Hurricane-forced upwelling and chlorophyll a enhancement within cold-core cyclones in the Gulf of Mexico. *Geo. Res. Lett.*, **32**, L18610.
- Ward, B. A., Friedrichs, M. A. M., Anderson, T. R. and Oschlies, A. (2010) Parameter optimisation techniques and the problem of underdetermination in marine biogeochemical models. *J. Mar. Syst.*, **81**, 34–43.
- Wawrik, B., Paul, J. H., Bronk, D. A., John, D. and Gray, M. (2004) High rates of ammonium recycling drive phytoplankton productivity in the offshore Mississippi River plume. *Aquat. Microb. Ecol.*, **35**, 175–184.
- Wright, S. (2008) *Chemtax version 1.95 for calculating the taxonomic composition of phytoplankton populations, Ver. 1, Australian Antarctic Data Centre*, doi: [10.4225/15/59fff1c5ea8fc](https://doi.org/10.4225/15/59fff1c5ea8fc), accessed 2020-06-01.
- Xiao, Y. and Friedrichs, M. A. M. (2014) Using biogeochemical data assimilation to assess the relative skill of multiple ecosystem models in the Mid-Atlantic Bight: effects of increasing the complexity of the planktonic food web. *Biogeosciences*, **11**, 3015–3030.
- Yool, A., Martin, A. P., Fernández, C. and Clark, D. R. (2007) The significance of nitrification for oceanic new production. *Nature*, **447**, 999–1002.
- Zubkov, M. V., Sleigh, M. A., Burkill, P. H. and Leakey, R. J. (2000) Picoplankton community structure on the Atlantic Meridional Transect: a comparison between seasons. *Prog. Oceanogr.*, **45**, 369–386.
- Zwirgmaier, K., Heywood, J. L., Chamberlain, K., Woodward, E. M. S., Zubkov, M. V. and Scanlan, D. J. (2007) Basin-scale distribution patterns of picocyanobacterial lineages in the Atlantic Ocean. *Environ. Microbiol.*, **9**, 1278–1290.
- Zwirgmaier, K., Jardillier, L., Ostrowski, M., Mazard, S., Garczarek, L., Vault, D., Not, F., Massana, R. et al. (2008) Global phylogeography of marine *Synechococcus* and *Prochlorococcus* reveals a distinct partitioning of lineages among oceanic biomes. *Environ. Microbiol.*, **10**, 147–161.